Environmental and Experimental Botany 248 (2026) 106406

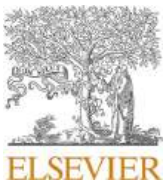

Contents lists available at ScienceDirect

Environmental and Experimental Botany

journal homepage: www.elsevier.com/locate/envexpbot

Research paper

Peroxisomal CATALASE2 positively regulates Arabidopsis lateral root development

Diego Piacentini [a,*], Alice Peduzzi [a], Simone D'Angeli [a], Federica Della Rovere [a], Francisco J. Corpas [b], Marta Rodríguez-Ruiz [b], Donato De Girolamo [a], Matteo Fedeli [a], Giulia Calonzi [a], Petre Dobrev [c], Barbora Svobodová [c], Maria Maddalena Altamura [a], Giuseppina Falasca [a]

[a] Department of Environmental Biology, Sapienza University of Rome, Italy
[b] Group of Antioxidants, Free Radicals and Nitric Oxide in Biotechnology, Food and Agriculture, Department of Stress, Development and Signaling in Plants, Estación Experimental del Zaidín, CSIC, C/Profesor Albareda 1, Granada E-18008, Spain
[c] Bioanalytical Service Laboratory, Institute of Experimental Botany of the Czech Academy of Sciences, Rozvojová 263, Prague 6 165 00, Czech Republic

ARTICLE INFO

Keywords:
Arabidopsis thaliana
Cadmium stress
CATALASE2
Nitro-oxidative stress
Cytokinin homeostasis
Root system architecture

ABSTRACT

Catalase (CAT) is one of the key enzymes in plant development and in the regulation of nitro-oxidative stress associated with the uncontrolled overproduction of reactive oxygen (ROS) and nitrogen species (RNS). Despite its well-established role in aerial organs, CAT functions in the root system remain underexplored. Using *Arabidopsis thaliana cat2–1*, defective in CAT2 and exhibiting reduced CAT activity, we demonstrated that CAT2 is directly involved in defining root architecture, particularly lateral root (LR) development under optimal growth conditions. Primary root (PR) and LR development were analysed in *cat2–1* through morpho-cyto-histological investigations, nitro-oxidative assays, and metabolomic analyses. To further investigate CAT2's role in root architecture, we exposed *cat2–1* to nitro-oxidative stress using 60 μM cadmium sulphate ($CdSO_4$). Results show that CAT2 is the main CAT isozyme in Arabidopsis root system. *cat2–1* showed inhibition of LR development and PR elongation, exacerbated by Cd. These defects were highlighted by cyto-histological analyses, revealing alterations in the division/differentiation patterns of pericycle cells competent for LR initiation as well as in meristematic cells of PR and LRs. *Cat2–1* root alterations were associated with an accumulation of *trans*-zeatin-type cytokinin and with changes in ROS- and, to a lesser extent, RNS-homeostasis. Loss of CAT2 function exacerbated some of the Cd-related alterations, particularly the disorganisation of cell division and differentiation patterns within root meristems, and ROS accumulation, supporting a positive role of CAT2 in root architecture. Our results demonstrate a new role for CAT2 *per se* in Arabidopsis root system development, beyond its involvement in regulating stress response processes.

1. Introduction

Catalase (CAT; EC 1.11.1.6) is considered one of the most important antioxidant enzymes regulating redox balance in plants, as it catalyses the breakdown of H_2O_2 into H_2O and O_2.

It is localised in the peroxisomal matrix, a major site of H_2O_2 production as a consequence of various physiological pathways, such as photorespiration, fatty acid β-oxidation, and superoxide dismutase (SOD; EC 1.15.1.1) activity, as well as of stress conditions (Kamada et al., 2003; Hernandez et al., 2010). Although CAT has a lower affinity for H_2O_2 than other enzymes, such as ascorbate peroxidase (APX; EC 1.11.1.11), its high turnover rate and accumulation within the peroxisomes makes it particularly efficient in H_2O_2 dismutation (Mhamdi et al., 2010).

In plants, CAT is encoded by small gene families, resulting in various isozymes, whose number differs among plant species (Palma et al., 2020). Additionally, within a plant species, the expression of different genes for CAT isozymes varies depending on the developmental stage, tissue or organ type, and environmental conditions (Frugoli et al., 1996; Kamada et al., 2003; Palma et al., 2020).

Accumulating evidence indicates that CAT is involved in several physiological processes, including leaf and cotyledon senescence,

* Corresponding author.
E-mail address: diego.piacentini@uniroma1.it (D. Piacentini).

https://doi.org/10.1016/j.envexpbot.2026.106406
Received 17 March 2026; Received in revised form 22 June 2026; Accepted 24 June 2026
Available online 25 June 2026

stomatal closure, seed viability and ageing (Ni and Trelease, 1991; Baker et al., 2023).

The importance of CAT in responses to environmental stress has also been highlighted in different plant species, both through the evaluation of changes in CAT activity or content and through studies on transgenic lines overexpressing *CAT* or mutants in one or more *CAT* genes (Guan et al., 2009; Zafar et al., 2020; Dai et al., 2020; Piacentini et al., 2020; Tyagi et al., 2021).

The *Arabidopsis thaliana* (L.) Heynh. *CAT* gene family comprises three members: *CAT1*, *CAT2* and *CAT3*. *CAT1* is primarily expressed in pollen and seeds, *CAT2* is the primary photorespiratory isozyme in photosynthetically active tissues and is also expressed, to a lesser extent, in roots and seeds, while *CAT3* is expressed in vascular tissues and senescent leaves (Frugoli et al., 1996; Su et al., 2018). Although the transcripts of the three *CATs* are detected in mature Arabidopsis leaves, with CAT3 and CAT2 more abundant than CAT1, each isozyme contributes to H_2O_2 scavenging in distinct physiological processes and developmental stages (Baker et al., 2023).

While *cat1* and *cat3* mutations do not significantly affect plant growth or total CAT activity in Arabidopsis, the *cat2* mutation causes reduced growth, pale-green leaves, and decreases in CAT activity of about 80% in leaves and 50% in roots. For this reason, this last isozyme is considered the primary CAT responsible for H_2O_2 degradation in Arabidopsis leaves and has therefore been used as a reference to investigate CAT function in plant physiological processes and stress responses (Bueso et al., 2007; Mhamdi et al., 2010; Yang et al., 2019).

In accordance with its function, CAT2 has been recognised as a key isozyme in plant responses to various stresses, including heat, salt, osmotic, and heavy metal stress, as well as in pathogen defence (Bueso et al., 2007; Yuan et al., 2017; Zhang et al., 2021; Ono et al., 2021).

Beyond stress responses, CAT2 is also crucial during early seedling development through its interaction with acyl-CoA oxidase (ACX), a key enzyme in peroxisomal fatty acid β-oxidation and a major source of H_2O_2 during early post-germination growth. This is particularly evident under sucrose-free conditions, in which peroxisomal fatty acid β-oxidation becomes the primary energy source, and ACX-mediated H_2O_2 production increases. Accordingly, many of the developmental defects observed in the *cat2* mutant are detectable under sucrose-free conditions and have been attributed to impaired fatty acid β-oxidation (Liu et al., 2017; Yang et al., 2019).

Consistently, the Arabidopsis *cat2–1* mutant shows reduced rosette leaf growth, which can be rescued under high CO_2 or irradiance conditions that reduce photorespiration, highlighting CAT2 as a key photorespiratory isozyme in the regulation of leaf redox state and growth (Queval et al., 2007).

CAT2 has also been identified as an important regulator of hormonal and metabolic responses. For example, in response to pathogen-induced salicylic acid (SA) accumulation, CAT2 activity is inhibited. This inhibition alters tryptophan (Trp) and jasmonic acid (JA) biosynthesis and leads to reduced indole−3-acetic acid (IAA) accumulation (Yuan et al., 2017). Metabolomic and transcriptomic analyses of the *cat2* mutant further revealed increased SA levels, accompanied by enhanced SA glycosylation mediated by specific UDP-glycosyltransferases, as well as activation of metabolic pathways that restrict the accumulation of bioactive jasmonate compounds (JAs) (Lelarge-Trouverie et al., 2023).

Furthermore, the most strongly repressed genes in the *cat2* mutant are those encoding auxin-responsive proteins of the SAUR (Small Auxin Up RNA) and AUX/IAA families (Bueso et al., 2007). Since these two families play opposite roles in auxin signaling, with SAUR proteins acting as positive mediators and AUX/IAA proteins as transcriptional repressors degraded upon auxin perception, their co-repression suggests a complex modulation of auxin responses by CAT2. Moreover, CAT-dependent H_2O_2 decomposition has been reported to be involved in IAA biosynthesis (Gao et al., 2014; Yuan et al., 2017; Li et al., 2021), further linking CAT2 activity to auxin homeostasis.

Similarly, CAT2 has been shown to regulate leaf morphology through H_2O_2-mediated transcriptional repression of auxin biosynthetic genes, thereby modulating auxin levels (Gao et al., 2014). Finally, Arabidopsis *cat2* mutants exhibit reduced ethylene synthesis and lower hormone sensitivity, which have been attributed to post-transcriptional modifications of key proteins, including oxidative modification of the ethylene receptor ETR1 (Bueso et al., 2007).

Despite its significance, research on CAT2 function has been largely focused on photosynthetic tissues, with limited attention to its potential involvement in the root system development, particularly from a morpho-anatomical and physiological perspective.

To date, only a limited number of studies have investigated the role of CAT2 in the root system, generally interpreting the effects of its absence as secondary or indirect consequences of altered CAT activity in aerial organs. For example, the reduction of primary root (PR) elongation observed in *cat2–1* under sucrose-free growth conditions has been interpreted as a consequence of altered photosynthetic processes (Yang et al., 2019).

Moreover, studies addressing CAT2 function in roots rarely consider the root system as an integrated structure comprising both embryonic and post-embryonic roots. At the same time, root redox status is often evaluated by focusing on a single ROS, whereas reactive nitrogen species (RNS), key components of cellular redox signalling, are largely overlooked (Corpas, 2016). This knowledge gap is relevant given the demonstrated crosstalk between ROS and RNS, and the fact that catalases undergo both ROS-mediated oxidation and RNS-mediated modifications, including nitration and S-nitrosation (Palma et al., 2020; González-Gordo et al., 2024)

A comprehensive analysis of CAT2 functions in the root system *per se*, under both physiological and stress conditions, is therefore needed, as this approach may provide novel insights into the role of catalase in root system architecture and redox regulation. The aim of the present study was therefore to investigate the role of the CAT2 isozyme in *Arabidopsis thaliana* root system development and in the regulation of root redox homeostasis.

To this end, Arabidopsis *wild-type* (Col−0) and the *cat2–1* mutant, characterised by a strong reduction in total CAT activity (Bueso et al., 2007), were grown in the presence or absence of a toxic level of Cd, given its well-established role as a stress agent that promotes the overproduction of ROS and RNS, particularly in roots (Gallego and Benavides, 2019; Romero-Puertas et al., 2019; Piacentini et al., 2021; Della Rovere et al., 2022). The root system of the Arabidopsis *cat2–1* was studied through a combination of morpho-cyto-histological analyses and assessment of ROS/RNS accumulation and spatial distribution. Additionally, targeted metabolite profiling of roots, including major plant hormones and other relevant metabolites, was performed.

Particular emphasis was placed on all components of the Arabidopsis root system, namely the PR, lateral root primordia (LRPs), and elongated lateral roots (LRs), with special focus on LRPs due to their high plasticity and responsiveness to environmental changes (Malamy, 2005; Altamura et al., 2023).

2. Materials and methods

2.1. Plant material and growth conditions

Arabidopsis thaliana (L.) Heynh. ecotype Columbia (Col−0, wild-type) and the *cat2–1* mutant (SALK_057998), in the Col−0 background (Alonso et al., 2003), were used in this study. Seeds of the *cat2–1* mutant, carrying a T-DNA insertion in the *CAT2* gene (*At4g35090*), were obtained from the Nottingham Arabidopsis Stock Centre (http://nasc.nott.ac.uk). Homozygosity of the *cat2–1* line was confirmed by PCR-based genotyping using two primer pairs listed in Supplementary Table 1, as detailed in Supplementary Methods 1 and Supplementary Figure 1. All subsequent analyses were performed on homozygous T1 seedlings. Seeds were surface sterilized by washing for 5 min in 70% (v/v) ethanol and 0.1% (w/v) SDS, followed by 20 min in 20% (v/v)

bleach and 0.1% (w/v) SDS, and were then rinsed four times with sterile water. Ten seeds per genotype were sown on square Petri dishes (245 mm × 245 mm) containing half-strength Murashige and Skoog medium (Murashige and Skoog, 1962; Duchefa Biochemie, The Netherlands) supplemented with 0.7% (w/v) sucrose, 0.7% (w/v) agar, and either 0 (Control) or 60 μM $CdSO_4$ (Merck, Italy). The pH was adjusted to 5.6–5.8. The $CdSO_4$ concentration was selected based on previous data obtained in Arabidopsis (Fattorini et al., 2017). Before light exposure, the sown seeds were kept in the dark at 8°C for 24 h for cold stratification. Seedlings were then grown vertically for 10 days under *in vitro* long-day conditions (16 h light/8 h dark) at 22 ± 2 °C with a light intensity of 100 μmol $m^{-2}s^{-1}$.

2.2. SDS-PAGE and Western blotting of CAT and CAT2

Root systems and green cotyledons from 10-day-old Arabidopsis seedlings were separately collected and homogenized in extraction buffer (1:1, w/v) containing 100 mM Tris-HCl (pH 8.0), 1 mM EDTA, 0.1% (v/v) Triton X−100, and 10% (v/v) glycerol. Homogenates were centrifuged at 27,000xg for 20 min at 4°C, and the resulting supernatants were used for all assays. Before SDS-PAGE, total protein concentration in each sample was determined in triplicate using the Bio-Rad protein assay solution (Bio-Rad Laboratories, Hercules, CA, U.S.A.), and the same amount of total protein (15 μg) was loaded in each lane. Thus, immunoblot signals were compared on an equal-total-protein-input basis across genotypes and treatments. Proteins were separated on 4–20% gradient precast polyacrylamide gels using a Mini-PROTEAN system (Bio-Rad, Hercules, CA, USA), according to Corpas et al. (2025). After electrophoresis, proteins were transferred onto 0.22 μm PVDF membranes using the Trans-Blot® Turbo™ Transfer System (Bio-Rad). Membranes were then probed with commercial rabbit polyclonal antibodies against Arabidopsis catalase (Agrisera, AS09 501; dilution 1:3000) and catalase−2 (Agrisera, AS21 4531; dilution 1:3000). Signals were detected using an HRP-conjugated goat anti-rabbit IgG secondary antibody (Bio-Rad) and Clarity™ Western ECL reagent (Bio-Rad). Chemiluminescent images were acquired with a Molecular Imager® Gel Doc™ XR system (Bio-Rad) as uncompressed grayscale TIFF files. Band intensities were quantified using ImageJ software (version 1.54d). Background subtraction was performed using the Rolling Ball algorithm, and bands were quantified using the Analyze Gels function by calculating the area under each density-profile peak. No additional normalization to a housekeeping protein or to post-transfer total-protein staining was performed.

2.3. Seed germination rate and root morphological analysis

Seed germination and root morphology analyses were performed on twenty-five seeds or seedlings per genotype and treatment. Germination rate was evaluated at 48 and 72 h and at 6 days after sowing, whereas primary root (PR) length was measured at 48 and 72 h, and at 6 and 10 days after sowing. Primary root length was quantified from digital images acquired directly from Petri dishes using a Canon EOS 2000 camera (Canon, Italy) and analysed with ImageJ v1.54d software (Schneider et al., 2012). Values were expressed as mean length (cm ± SEM). The total number of lateral root primordia (LRPs) and mature lateral roots (LRs) was determined 10 days after sowing by observing each root system under a Leica DMRB microscope (Leica Microsystems, UK) and values were expressed as means (± SEM). Finally, the LR density was calculated for each seedling as the total number of LRPs plus LRs per cm of PR and expressed as a mean (± SEM). Individual values and mean ± standard deviation (SD) for root morphological traits are provided in Supplementary Figure 2.

2.4. Root-targeted metabolite quantification

Root-targeted metabolite quantification was performed on three biological replicates per genotype and treatment, each consisting of 150 seedlings, following Schmidt et al. (2024). Frozen root samples were extracted with 100 μL of 1 M formic acid after the addition of isotope-labelled internal standards. After centrifugation at 30,000×g at 4 °C, the supernatants were purified using Oasis HLB solid-phase extraction 96-well plates (10 mg per well; Waters, Milford, MA, USA), previously conditioned with acetonitrile and 1 M formic acid. The plates were washed three times with water, and the metabolites were eluted with 50% acetonitrile in water. Chromatographic separation was performed on a Kinetex EVO C18 column (2.6 μm, 150 × 2.1 mm; Phenomenex, Torrance, CA, USA) using 5 mM ammonium acetate and 2 μM medronic acid in water as mobile phase A and acetonitrile (95:5, v/v) as mobile phase B. The gradient was as follows: 5% B at 0 min, 5–7% B from 0.1 to 5 min, 10–35% B from 5.1 to 12 min, and 35–100% B from 12 to 13 min, followed by a 1-min hold at 100% B and re-equilibration at the initial conditions. Analyses were performed using a 1290 Infinity II UHPLC system coupled to a 6495 Triple Quadrupole Mass Spectrometer (Agilent, Santa Clara, CA, USA). Metabolites were detected by targeted analysis in multiple reaction monitoring mode using predefined compound-specific transitions. Data were acquired and processed using MassHunter software B.08 (Agilent), with peak integration performed using the Agile2 algorithm followed by manual verification. Absolute quantification was carried out by isotope dilution using isotope-labelled internal standards, and metabolite contents were normalised to sample fresh weight. The targeted metabolites included major classes of plant hormones, such as abscisic acid (ABA), jasmonates, auxins, cytokinins and related compounds, as well as phenolic metabolites. Only selected representative metabolites are reported, and their contents, expressed as pmol g^{-1} FW, are presented as means ± SEM. To highlight variations in overall metabolite profiles between genotypes and/or treatments, mean values for each hormone were also Z-normalised and plotted as a heatmap. Only metabolites showing at least one statistically significant difference, either between treatments within the same genotype or between genotypes within the same treatment, were included in the heatmap.

2.5. Root ROS and RNS analyses

ROS were analysed by evaluating total ROS levels as well as individual species, including hydrogen peroxide (H_2O_2) and superoxide anion ($O_2^{\bullet-}$), through their distribution and accumulation in roots. Nitric oxide ($^{\bullet}NO$) and peroxynitrite ($ONOO^-$) levels and distribution were also analysed. The distribution and accumulation of each ROS and RNS were analysed in the root systems of five seedlings per genotype and treatment. H_2O_2 was detected using the 3,3-diaminobenzidine (DAB; Sigma-Aldrich) assay, following the procedure of Piacentini et al. (2020) with slight modifications. Root systems were vacuum-infiltrated for 5 min and then incubated for 1 h at room temperature (RT) in complete darkness in 1% DAB prepared in Milli-Q water. The pH of the solution was adjusted to 7.0 with 200 mM Na_2HPO_4. $O_2^{\bullet-}$ detection was performed using the nitroblue tetrazolium (NBT; Roche Diagnostics Corp., GmbH, Germany) assay. Root systems were incubated for 30 min in the dark at RT in a solution containing 0.5 mg L^{-1} of NBT in 10 mM Tris-HCl buffer (pH 7.40 ± 0.05; Merck, Italy). After incubation, roots were thoroughly washed with Milli-Q water to stop the reaction and observed under a Leica DMRB brightfield microscope. Images were acquired with an Optika digital camera (C-P20CC, Optika, Italy) and processed with OPTIKA PROView image analysis software (version May 2021). Superoxide anion level was also quantified spectrophotometrically at 630 nm using a Shimadzu UV−1280 spectrophotometer (Shimadzu, Japan), using three aliquots (~30 mg each) per genotype and treatment collected from 25 seedlings (Vaccarella et al., 2023). Total ROS content was analysed by incubating the root systems for 30 min at 25°C in complete darkness in 20 mM HEPES-NaOH buffer (pH 7.4) containing the general oxidative stress indicator 5-(and−6)-chloromethyl−2′, 7′-dichlorodihydrofluorescein diacetate, acetyl ester (CM-H_2DCFDA,

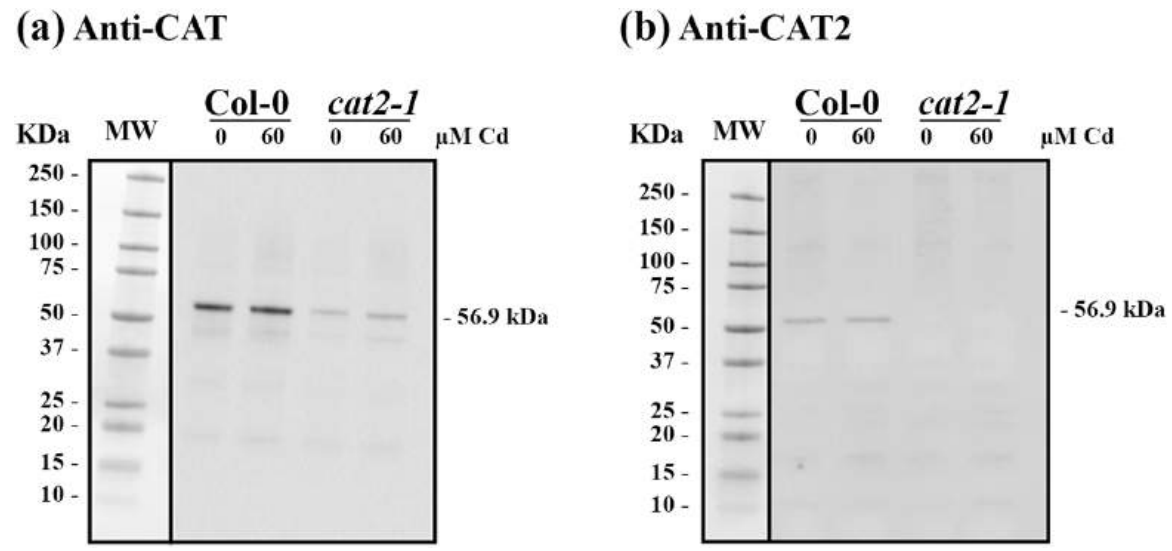

Fig. 1. Immunodetection of CATALASE (CAT) proteins in the roots of 10-day-old Col−0 and *cat2−1* seedlings grown in the presence or absence of 60 µM $CdSO_4$ (60 µM Cd). (a) Representative immunoblot obtained using an antibody recognising the three Arabidopsis CAT isozymes. (b) Representative immunoblot obtained using a CAT2-specific antibody. Equal amounts of total protein (15 µg per lane) were loaded.

Thermo Fisher Scientific, USA). For •NO and $ONOO^-$ detection, root systems were incubated at 25°C in complete darkness for 30 min and 60 min, respectively, in solutions containing either 10 µM 4-Amino−5-Methylamino−2′,7′-Difluorofluorescein Diacetate (DAF-FM diacetate, Thermo Fisher Scientific, USA) in 20 mM HEPES-NaOH buffer (pH 7.4) or 10 µM Aminophenyl fluorescein (APF, Thermo Fisher Scientific, USA) in 10 mM Tris-HCl buffer (pH 7.4). After incubation, root systems were rinsed three times with the corresponding buffer to remove excess probe. Total ROS, •NO and $ONOO^-$ fluorescence signals were analysed using an Axio Imager M2 microscope (Zeiss, Germany) equipped with an LSM 900 confocal unit and a 488 nm, 10 mW solid-state laser, with emission collected in a 500–530 nm band. Longitudinal root images were acquired at different magnifications with a minimum resolution of 1100 × 1100 pixels using Zeiss ZEN 3.1 software.

Fluorescence signals were quantified using ImageJ v1.54d software by converting images to grayscale and assigning each pixel an intensity value ranging from 0 (black) to 255 (white) arbitrary units (AUs). To enhance visualisation without altering the original intensity values, •NO and $ONOO^-$ images were additionally displayed using the Look-Up Tables (LUTs) function in ImageJ (Schneider et al., 2012), whereas ROS images were false-colored red using the same software.

2.6. Cyto-histological analyses

The primary root (PR) region, including lateral root primordia (LRPs) and mature lateral roots (LRs), from five seedlings per genotype and treatment was collected for histological analysis. In Control seedlings, the apical 3 cm of PRs were excised, whereas in Cd-treated seedlings, in which PR length was markedly reduced, the entire primary root was collected. Samples were fixed in 70% (v/v) ethanol, dehydrated through a graded ethanol series, embedded in Technovit 7100 resin (Heraeus Kulzer, Germany), and longitudinally sectioned at 8 µm using an Epredia HM355S microtome (Epredia, Italy). Sections were stained with 0.05% toluidine blue and observed under a Leica DMRB brightfield microscope (Leica Microsystems, Germany). Pericycle cell proliferation and division planes were evaluated along the PR axis. Meristem organization and cell differentiation were inferred from cell size, degree of vacuolisation, and establishment of the quiescent centre (QC).

2.7. Statistical analysis

All experiments were performed in three independent biological replicates. Quantitative data were analysed by one-way or two-way ANOVA, followed by Tukey's post hoc test ($P < 0.05$), after verification of normality with Shapiro–Wilk's test and homogeneity of variances with Bartlett's test. Germination data were analysed using the chi-square (χ^2) test. All statistical analyses and data visualisation were performed using GraphPad Prism software (Version 8.0.2; GraphPad Software, USA).

3. Results

3.1. The CAT2 isozyme is present in Arabidopsis roots, and its content is slightly affected by Cd treatment

A PCR-based validation of *cat2–1* homozygosity was preliminarily performed using genomic DNA from Col−0 and *cat2–1* seedlings (Supplementary Methods 1 and Supplementary Fig. 1). Subsequently, the relative abundance of total CAT-immunoreactive proteins and CAT2 was assessed in the root systems of Col−0 and *cat2–1* seedlings using a general anti-CAT antibody recognising all three CAT isozymes and a CAT2-specific antibody, respectively (Fig. 1). The same analyses were also performed on green cotyledons (Supplementary Fig. 3).

In Col−0 roots, a clear CAT-immunoreactive signal was detected, although it was lower than that observed in green cotyledons (Fig. 1a; Supplementary Fig. 3a). In *cat2–1* roots, the signal detected with the general anti-CAT antibody was markedly lower than in Col−0. Since no CAT2-specific signal was detected in the mutant, the residual signal obtained with the general antibody can be attributed to CAT1 and/or CAT3. The reproducible reduction in CAT immunoreactivity observed in *cat2–1* suggests that CAT2 may represent a major contributor to the overall CAT protein pool in Arabidopsis roots. Densitometric analysis indicated that Cd exposure caused only a modest increase in the relative total CAT-immunoreactive signal in both *Col−0* and *cat2–1* compared with the respective Controls (approximately 17%; Fig. 1a). Similarly, the CAT2-specific antibody detected a distinct band in Col−0 roots, whose relative intensity was only slightly higher following Cd exposure, with an increase of approximately 4% (Fig. 1b). No CAT2-specific signal was detected in *cat2–1* roots under either growth condition, confirming the absence of detectable CAT2 protein in the mutant.

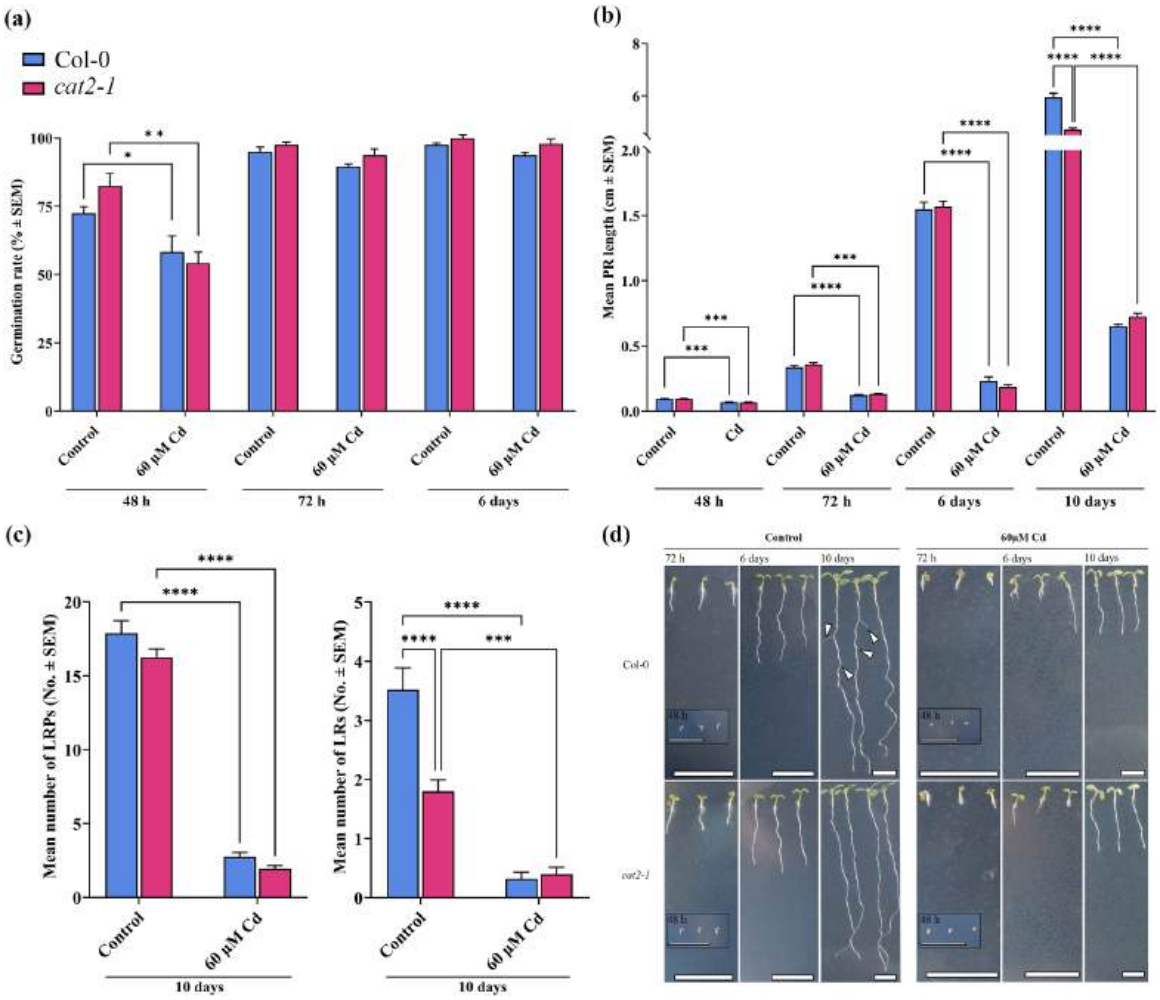

Fig. 2. Germination rate (a) and root morphological analyses (b-d) of Col−0 and *cat2−1* seedlings grown in the presence or absence of 60 µM $CdSO_4$ (60 µM Cd). (a) Germination rate (± SEM) at 48 h, 72 h, and 6 days after sowing. (b) Mean primary root (PR) length (± SEM) at 48 h, 72 h, 6 days, and 10 days after sowing. (c) Mean number of lateral root primordia (LRPs) (± SEM) and mean number of mature lateral roots (LRs) (± SEM) at 10 days from sowing. Statistical comparisons were performed between treatments within the same genotype and time point and between genotypes within the same treatment and time point. *, $P < 0.05$; **, $P < 0.01$; ***, $P < 0.001$; ****, $P < 0.0001$. Data are from the first biological replicate. N = 25. (d) Representative images of Col−0 and *cat2−1* seedlings grown with or without 60 µM Cd after 48 h (insets), 72 h, 6 days and 10 days after sowing. Arrowheads indicate LRs in Col−0 under Control treatment. Scale bars = 1 cm.

3.2. The cat2 mutation impairs root system architecture and this effect is hidden by Cd stress

The germination rate was comparable between Col−0 and *cat2–1* at all the observed time points (i.e. 48 h, 72 h, 6 days after sowing), indicating that the absence of CAT2 does not affect Arabidopsis germination (Fig. 2a). Cadmium treatment caused a delay in seed germination in both genotypes, as a significantly lower germination rate was observed at 48 h compared with the Control. However, this delay was fully recovered at later time points, when germination rates became comparable to those of the Control (Fig. 2a). Under Control conditions, PR length was comparable between the two genotypes at all time points, except at day 10 after sowing, when *cat2–1* showed a PR length approximately 21% shorter than that of Col−0 (Fig. 2b,d). This reduction was not caused by a germination delay induced by the mutation (Fig. 2a) but rather appeared to result from an arrest in PR elongation.

Cadmium exposure significantly reduced PR length with a comparable effect in Col−0 and *cat2–1*, as early as 48 h after treatment. Specifically, relative to the Control, the reduction in PR length under Cd exposure was approximately 27%, 63%, 85%, and 90% at 48 h, 72 h, 6 days, and 10 days after sowing, respectively (Fig. 2b,d). Since the mutation-induced phenotype in PRs was detected specifically 10 days after sowing, the number of LRPs and LRs was also quantified at this time point (Fig. 2c), and their density determined (Supplementary Fig. 4). Regarding the LRPs, their mean number was comparable between Col−0 and *cat2–1* seedlings under Control conditions.

In contrast, the mutant exhibited a significant reduction in the mean number of LRs (arrowheads in Col−0), by 48.6% compared to Col−0 (Fig. 2c-d), despite both genotypes showing a comparable density of LRPs plus LRs (Supplementary Fig. 4). Cadmium treatment exerted a strong and similar negative effect on LR formation in both *cat2–1* and Col−0, significantly reducing the mean number of LRPs by 88% and 85% respectively, and that of LRs by 78% and 90% (Fig. 2c,d). Collectively, these results suggest that CAT2 contributes to the regulation of root system architecture under physiological conditions, particularly by affecting LRP development and confirm Cd as a strong stressor for root system development, with detectable effects already after 48 h of exposure.

3.3. The cat2 mutation and the Cd stress alter the hormonal and phenolic metabolism in Arabidopsis roots

The metabolite profiling of the roots of 10-day-old Col−0 and *cat2–1* seedlings, either exposed or not to Cd, highlighted a total of detected and

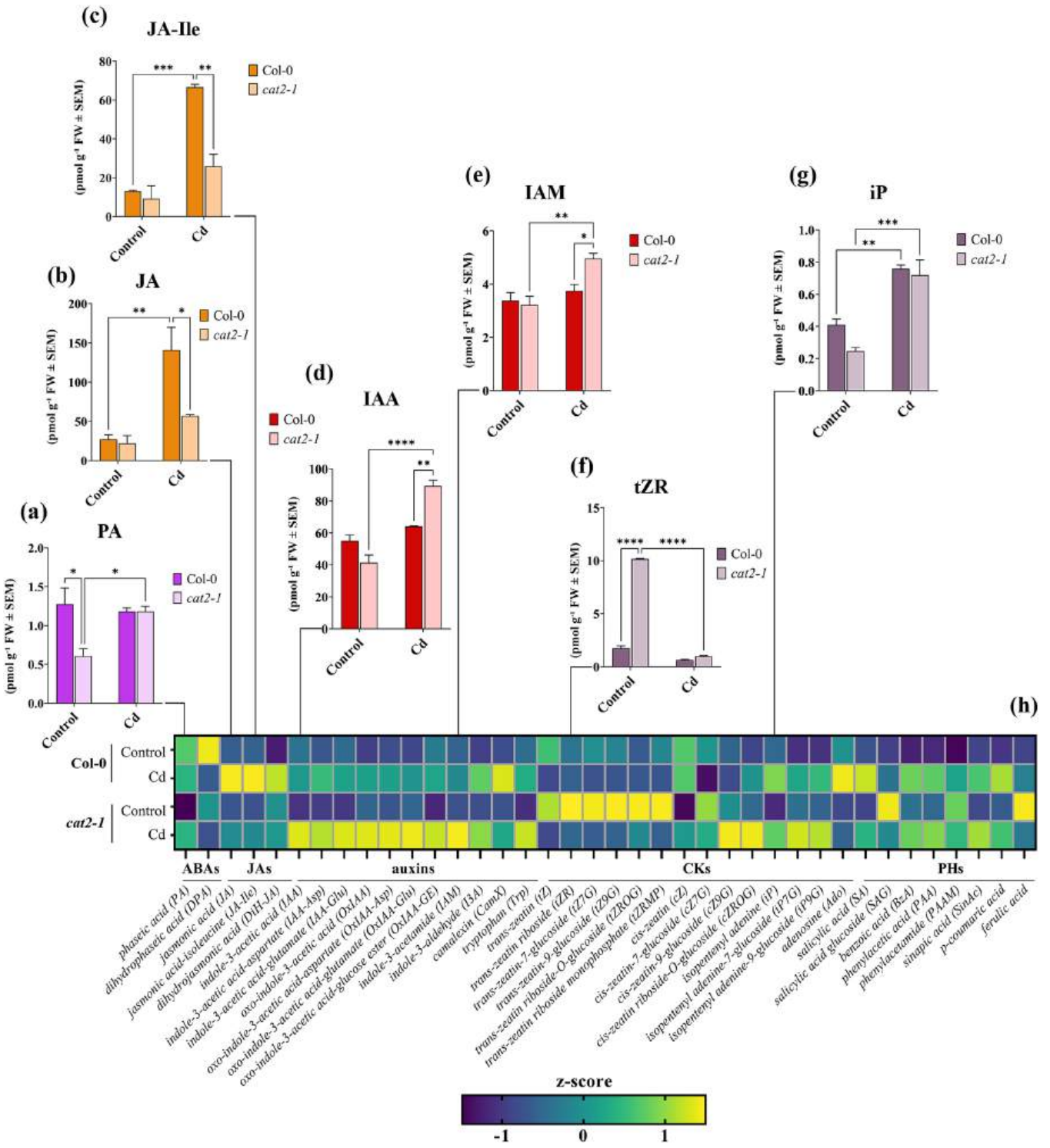

Fig. 3. (a-g) Bar plots of the mean concentrations (pmol g^{-1} FW ± SEM) of the most representative bioactive metabolites, belonging to ABAs (dark and light purple), JAs (dark and light orange), auxins (dark and light red), or CKs (dark and light grey) classes and present in the root system of 10-day-old Col−0 and *cat2−1* seedlings grown in the presence or absence of 60 μM $CdSO_4$ (Cd). Statistical comparisons were performed between treatments within the same genotype and between genotypes within the same treatment. *, $P < 0.05$; **, $P < 0.01$; ***, $P < 0.001$; ****, $P < 0.0001$. N = 3. (h) Heatmap of the targeted metabolites. The colour scale represents z-normalised values of each metabolite across samples, with yellow indicating higher concentrations and blue indicating lower relative concentrations. Abbreviations: ABAs, abscisic acid and related compounds; CKs, cytokinins; IAA, indole−3-acetic acid; IAM, indole−3-acetamide; JAs, jasmonates; JA, jasmonic acid; JA-Ile, jasmonoyl-L-isoleucine; PA, phaseic acid; PHs, phenolic metabolites; iP, isopentenyl adenine; tZR, trans-zeatin riboside.

quantified 53 compounds, including active hormones, their precursors and conjugated or catabolized forms, belonging to five classes: abscisic acids (ABAs), jasmonates (JAs), auxins, cytokinins (CKs) and phenolic compounds (PHs). Overall, both the mutation and Cd significantly affected the levels of 38 of the highlighted metabolites, often resulting in their upregulation, with some combined effects observed, particularly for auxins and *cis*-zeatin-type CKs (Fig. 3).

The compounds exhibiting the most significant changes among

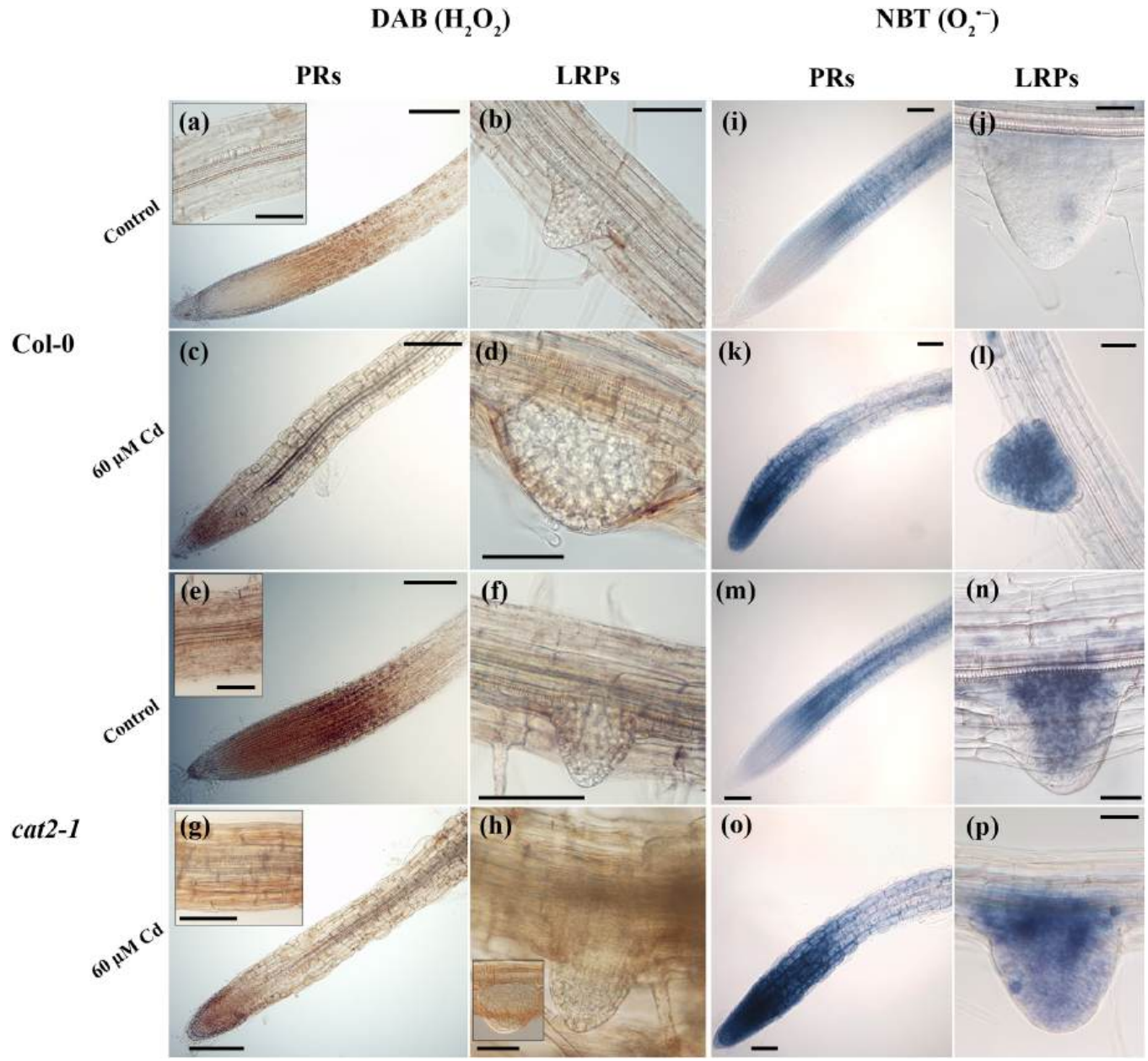

Fig. 4. Representative images of DAB (a-h) and NBT (i-p) histochemical staining, showing H_2O_2 (dark brown) and $O_2^{\bullet-}$ accumulation (dark blue), respectively, in the primary roots (PRs) and lateral root primordia (LRPs) of 10-day-old Col−0 and *cat2−1* seedlings grown in the presence or absence of 60 µM $CdSO_4$ (60 µM Cd). Images are representative of three biological replicates. The arrowhead in (a) indicates signal presence in the PR elongation zone, arrowhead in (b) indicate signal presence in the LRP basal portion, in (d) signal presence in the LRP protoderm, in (e) signal presence in the PR meristem and elongation zone, in (g) signal presence in PR meristem, in (k) and (m) signal presence in the PR inner tissues and in (l) signal absence in the LRP protoderm. Bars = 50 µm (d), 100 µm (b,c,f,h-p insets in a,e,g, h), 200 µm (a,e,g).

genotypes or treatments are described below (Fig. 3), with additional details provided in Supplementary Figure 5.

The ABA metabolites, particularly phaseic acid (PA), accumulated in the roots of Col−0 at higher concentrations than in those of *cat2–1* (Fig. 3a). However, Cd induced a significant increase in PA in the mutant, which reached levels comparable to the wild-type (Fig. 3a,h). Jasmonic acid (JA) and the jasmonate–isoleucine conjugate (JA-Ile) exhibited similar levels in both genotypes under Control conditions (Fig. 3b,c), and Cd significantly increased their levels, but only in Col−0 (Fig. 3b,c,h). Similar to JAs, auxins (including bioactive forms, precursors, catabolic products, and amino acid conjugates) were present at comparable levels in the two genotypes under Control conditions, as exemplified by indole−3-acetic acid (IAA) and indole−3-acetamide (IAM) (Fig. 3d,e,h). However, Cd treatment resulted in significantly greater accumulation of these molecules in *cat2–1* roots than in wild-type roots (Fig. 3d,e). Cytokinin metabolites, particularly of the *trans*-zeatin (tZ)-types, accumulated to higher levels in *cat2–1* than in the wild-type, as reported for *t*Z-riboside (*t*ZR) (Fig. 3 f,h). However, their levels markedly decreased in the mutant roots under Cd exposure, becoming negligible as in the wild-type under the same treatment (Fig. 3 f,h). By contrast, cZ-type CKs were at comparable levels between the two genotypes in Control conditions, with a preferential increase observed in *cat2–1* after Cd treatment (Fig. 3 h). Other cytokinins, such as the bioactive isopentenyl adenine (iP), were also present at comparable levels in both genotypes in the absence of Cd-stress and showed a similarly significant increase upon Cd exposure (Fig. 3 g,h).

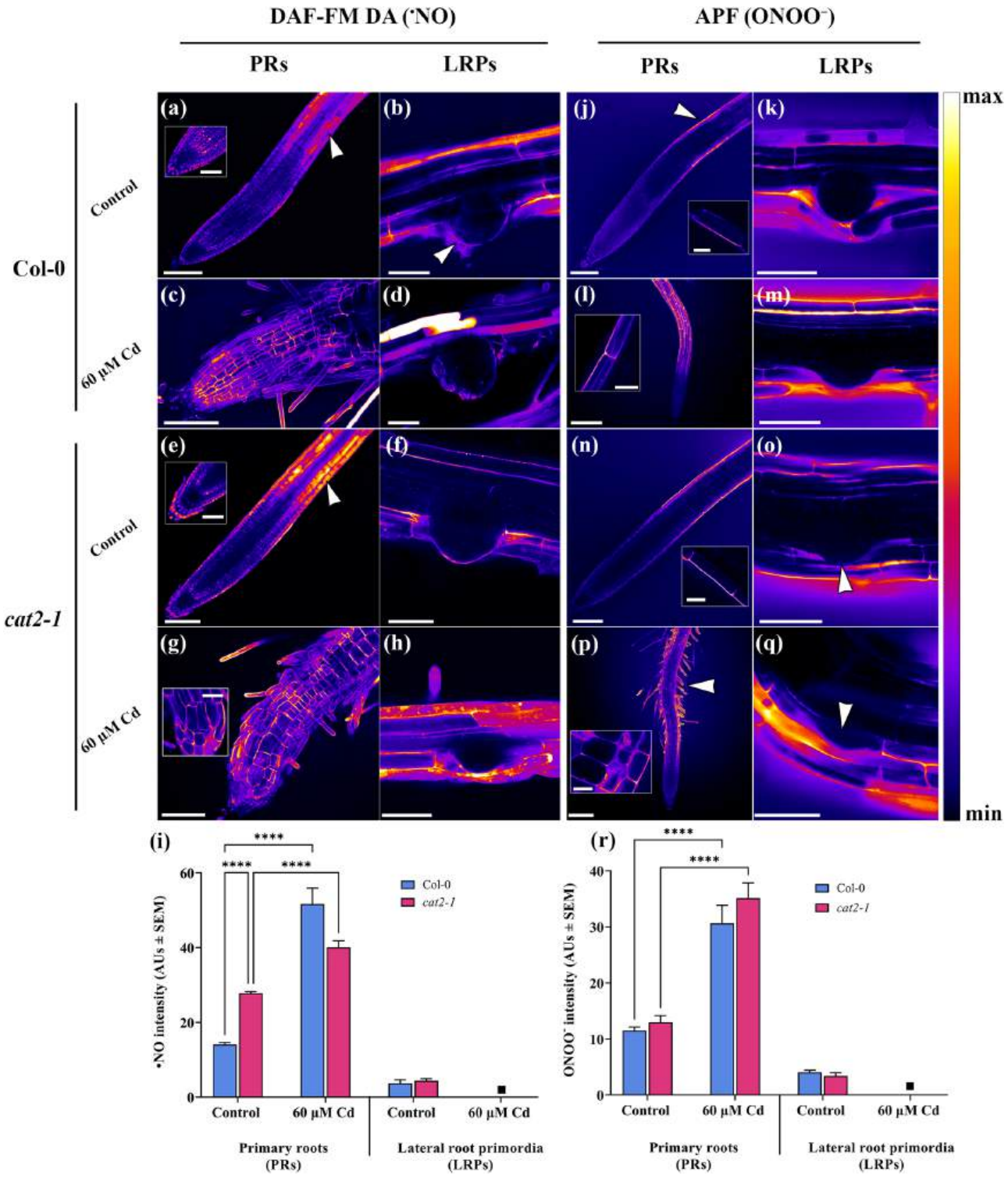

Fig. 5. Representative confocal microscopy images showing nitric oxide (•NO) (a-h) and peroxynitrite ($ONOO^-$) (j-q) signals in the primary roots (PRs) and lateral root primordia (LRPs) of 10-day-old Col−0 and *cat2−1* seedlings grown in the presence or absence of 60 µM $CdSO_4$ (60 µM Cd) and treated with the fluorescence probe DAF-FM DA or with APF, respectively. The colour scale bar on the left indicates fluorescence intensity (min-max) according to the applied LUT. Arrowheads in (a) and (e) indicate signal presence in the PR elongation zone, in (b) and (j) signal presence in the PR epidermis, in (p) signal presence in the PR root hairs and in (o) and (q) signal absence in a LRP. (i,r) Bar plots showing the mean values of the •NO (i) and $ONOO^-$ (r) fluorescence signals, expressed in arbitrary units (AUs ± SEM). Statistical comparisons were performed between treatments within the same genotype and between genotypes within the same treatment. ****, $P < 0.0001$. The ■ symbol indicates that fluorescence quantification was not performed due to the limited number of LRPs. Bars = 25 µm (insets in g,j,l,n,p); 50 µm (inset in a, b,d,inset in e,f,h,k,m,o,q); 100 µm (a,c,e,g,j,n); 200 µm (l,p). N = 15.

Finally, some PHs, such as salicylic acid glucoside (SAG), phenylacetamide (PAAM) and ferulic acid, were more abundant in the roots of *cat2–1* compared to Col−0 under Control conditions. Cadmium treatment differentially modulated their levels, increasing them in Col−0 while decreasing them in the mutant, ultimately resulting in comparable concentrations between the two genotypes (Fig. 3 h; Supplementary Fig. 5).

Taken together, these results indicate that both the loss of CATALASE2 and the Cd exposure deeply alter the hormonal and phenolic metabolism of the Arabidopsis roots. In particular, *cat2–1* mutation significantly impacts cytokinin metabolism, especially that of tZ-type compounds, whereas Cd primarily affects the levels of JAs and certain phenolic compounds.

The combined effects of the mutation and Cd exposure resulted in hormone-specific responses, with some effects being synergistic, such as the increase in IAM levels, and others antagonistic, such as the decrease in JA levels. These findings suggest a complex cross talk among hormonal pathways in response to CAT2 loss and Cd-induced stress.

3.4. CAT2 affects the accumulation and spatial distribution of ROS in the root system, with differences between primary roots and lateral root primordia

To further investigate the effects of the *cat2* mutation on PR development and on LRP formation, the accumulation and spatial distribution of the major ROS, i.e., H_2O_2 and $O_2^{\bullet-}$, were analysed in both genotypes in the presence or absence of Cd (Fig. 4; Supplementary Figs. 6 and 7).

In Col−0 roots under Control conditions, the H_2O_2 signal, detected by DAB staining as a dark brown cellular precipitate, was weakly detectable and primarily localised in the elongation zone of the PR (Fig. 4a, arrowhead), whereas no signal was detected in the differentiated region (Fig. 4a, inset). In LRPs, H_2O_2 staining was not detected, except for a faint signal at the basal region (Fig. 4b, arrowhead). Upon Cd exposure, the H_2O_2 signal in Col−0 PR was more evident and was detected mainly in the root meristem, while it was not observed in the elongation zone (Fig. 4c). Furthermore, Cd treatment induced H_2O_2 staining in the LRP protoderm (Fig. 4d, arrowheads). In *cat2–1* seedlings not exposed to Cd, the H_2O_2 signal was more readily detectable than in Col−0 and was detected in both the PR root meristem and elongation zone (Fig. 4e, arrowheads), extending at lower intensity into the differentiation region (Fig. 4e, inset). Similar to Col−0, H_2O_2 staining in *cat2–1* LRPs was mainly confined to the basal region. However, unlike in Col−0, the signal was more intense and slightly extended toward the margins of the primordium (Fig. 4f). Cadmium exposure resulted in an H_2O_2 localisation pattern in *cat2–1* similar to that observed in Col−0 under the same conditions, though *cat2–1* exhibited more evident staining, particularly in the PR meristem and in the basal portion of the LRPs (Fig. 4g, arrowhead; Fig. 4h, inset). However, unlike Col−0, H_2O_2 staining was also detectable in the differentiated region of the PRs (Fig. 4g, inset).

The $O_2^{\bullet-}$ signal, detected by NBT staining through formazan formation, showed a different distribution pattern. In Col−0 roots not exposed to Cd, $O_2^{\bullet-}$ staining was weakly detectable and mainly localised in the elongation and differentiation zones of the PR (Fig. 4i). No $O_2^{\bullet-}$ accumulation was observed in LRPs, except for a limited signal in their basal portion (Fig. 4j). Cadmium exposure resulted in a more evident $O_2^{\bullet-}$ signal in both PRs and LRPs of Col−0. Specifically, in the PRs, the signal was detected in the meristematic region and in the inner tissues of the elongation zone (Fig. 4k, arrowhead), whereas in LRPs it extended throughout the entire structure, except for the protoderm (Fig. 4l, arrowheads). In *cat2–1* seedlings not exposed to Cd, $O_2^{\bullet-}$ staining was more evident in both PRs and LRPs than in Col−0 (Fig. 4m-n and i-j in comparison). In particular, in the PRs, the signal was mainly observed in the elongation zone (Fig. 4m, arrowhead), gradually decreased towards the differentiated region, and remained detectable in the stele (Fig. 4m).

In contrast, LRPs showed a variable pattern of $O_2^{\bullet-}$ distribution: in some primordia, the signal extended throughout the entire structure; in others, it was restricted to the central cells (Fig. 4n), and in a few cases it was not detected. As in Col−0, Cd treatment in *cat2–1* was associated with a broader and more evident $O_2^{\bullet-}$ staining pattern in both PRs and LRPs than under Control conditions. Notably, in the mutant, a strong $O_2^{\bullet-}$ signal was detected in the meristematic regions of the PRs, and in the entire LRPs, mainly their basal part (Fig. 4o,p).

Consistent with these histochemical observations, absorption spectra of formazan obtained from extracts of Col−0 and *cat2–1* seedlings showed a 49% higher $O_2^{\bullet-}$ signal in *cat2–1* than in Col−0 under Control conditions. Cd-treatment further increased $O_2^{\bullet-}$ accumulation by 29% in Col−0 seedlings only (Supplementary Fig. 6).

To further investigate ROS distribution and accumulation in PRs and LRPs of both genotypes, root systems were also analysed with the ROS-sensitive fluorescent probe CM-H_2DCFDA by confocal laser scanning microscopy (Supplementary Fig. 7). This analysis, together with fluorescence quantification, supported the presence of a broader ROS-associated signal in *cat2–1* roots than in Col−0, particularly in PRs and, to a lesser extent, in LRPs, with the most extensive signal observed after Cd treatment.

Taken together, these results indicate that CAT2 influences ROS distribution patterns in Arabidopsis roots, with differences between PRs and LRPs. Cadmium treatment was associated with changes in ROS localisation in both genotypes, particularly in the apical region of the PR, and with distinct distribution patterns depending on the ROS considered. Quantitative analyses further supported genotype- and treatment-dependent differences in ROS accumulation. In addition, Cd-induced changes in ROS-related signals were more pronounced in *cat2–1* than in Col−0.

3.5. The cat2 mutation increases nitric oxide ($^{\bullet}$NO) accumulation in primary roots but not in lateral root primordia

Using fluorescent probes and confocal microscopy, we evaluated the localisation and relative accumulation of $^{\bullet}$NO and $ONOO^-$ in the roots of Col−0 and *cat2–1* seedlings, either exposed or not to Cd. In Col−0 PRs not exposed to Cd, the $^{\bullet}$NO signal was mainly localised in the epidermis and cortical parenchyma of the elongation and differentiation zones, with a weak fluorescence also observed in the basal part of the meristem and in the root cap (Fig. 5a, inset and arrowhead). In LRPs, the $^{\bullet}$NO signal was very weak and confined to the protoderm (Fig. 5b, arrowhead).

Cadmium treatment markedly increased the $^{\bullet}$NO signal compared with the Control, particularly in the outer tissues of the PR apices, without significantly affecting either its intensity or spatial distribution in LRPs (Fig. 5c,d,i).

In *cat2–1* PRs not exposed to Cd, the $^{\bullet}$NO fluorescence was significantly higher than in Col−0, while maintaining a similar localisation pattern, except for a more evident signal in the root cap (Fig. 5e, inset and arrowhead). In contrast, LRPs displayed a $^{\bullet}$NO-related signal pattern comparable to that observed in Col−0 (Fig. 5f,i). Cadmium treatment further increased the $^{\bullet}$NO fluorescence in *cat2–1* PRs, whereas no significant changes were detected in LRPs (Fig. 5g,h,i).

In Col−0 PRs under Control conditions, the $ONOO^-$ signal was low and mainly localised in the epidermis of the elongation zone (Fig. 5j, inset and arrowhead), whereas it was almost undetectable in LRPs (Fig. 5k). Cadmium treatment significantly increased $ONOO^-$ fluorescence in the outer tissues of Col−0 PRs, whereas LRPs were unaffected (Fig. 5l, inset; Fig. 5m,r). Under Control conditions, *cat2–1* PRs showed similarly low $ONOO^-$ signal intensity and localisation as Col−0 PRs, and the same undetectable signal in LRPs (Fig. 5n, inset; Fig. 5o,arrowhead, r). Upon Cd exposure, *cat2–1* PRs exhibited a significant increase in $ONOO^-$ fluorescence, comparable in intensity to that observed in Col−0 PRs, but with a broader spatial distribution extending to root hairs and cortical parenchyma cells (Fig. 5p, inset and arrowhead; Fig. 5r). In contrast, the $ONOO^-$ signal remained low in LRPs (Fig. 5q, arrowhead).

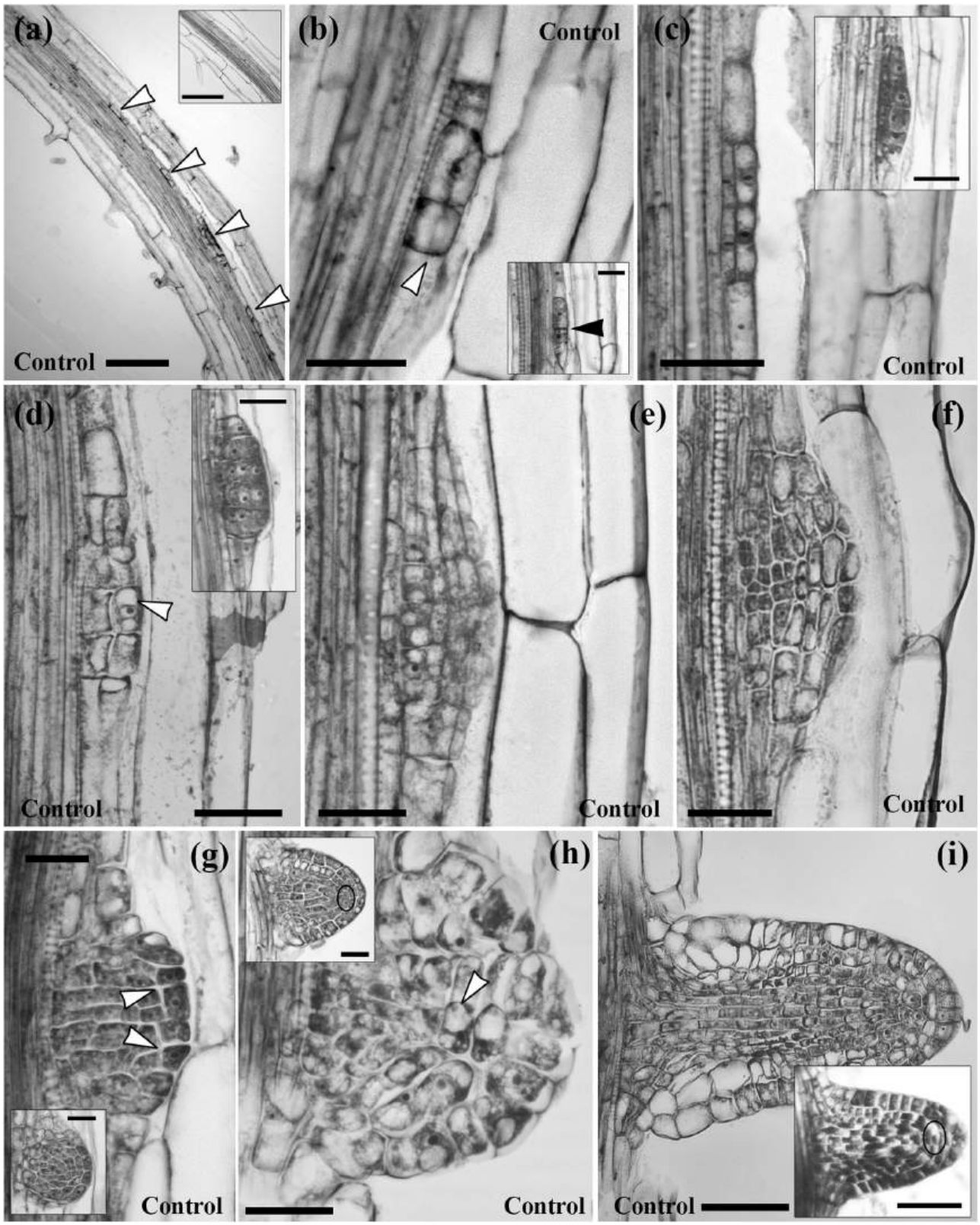

Fig. 6. Histological images of lateral root primordia (LRPs) at different developmental stages (a-i) and of an emerging lateral root (LR) in 10-day-old *cat2−1* seedlings grown in the absence of 60 μM $CdSO_4$ (Control). Main panels show *cat2−1* LRPs; insets show Col−0 LRPs at the same developmental stages. Insets show the regular PR pericycle divisions (a-b), LRPs (c-h) or LR (i) of Col−0 seedlings. Images are representative of three biological replicates. Arrowheads in (a) indicate an anomalous cell proliferation activity, in (b) and (g) anomalous cell divisions and in (d) and (h) large vacuoles in prematurely differentiated cells. The black arrowhead in the inset in (b) indicates regular anticlinal cell divisions. Black circles in inset in (h) and in (i) mark the regular quiescent centre cells. Bars = 25 μm (b-h and insets); 50 μm (inset in i);100 μm (a,inset,**i**).

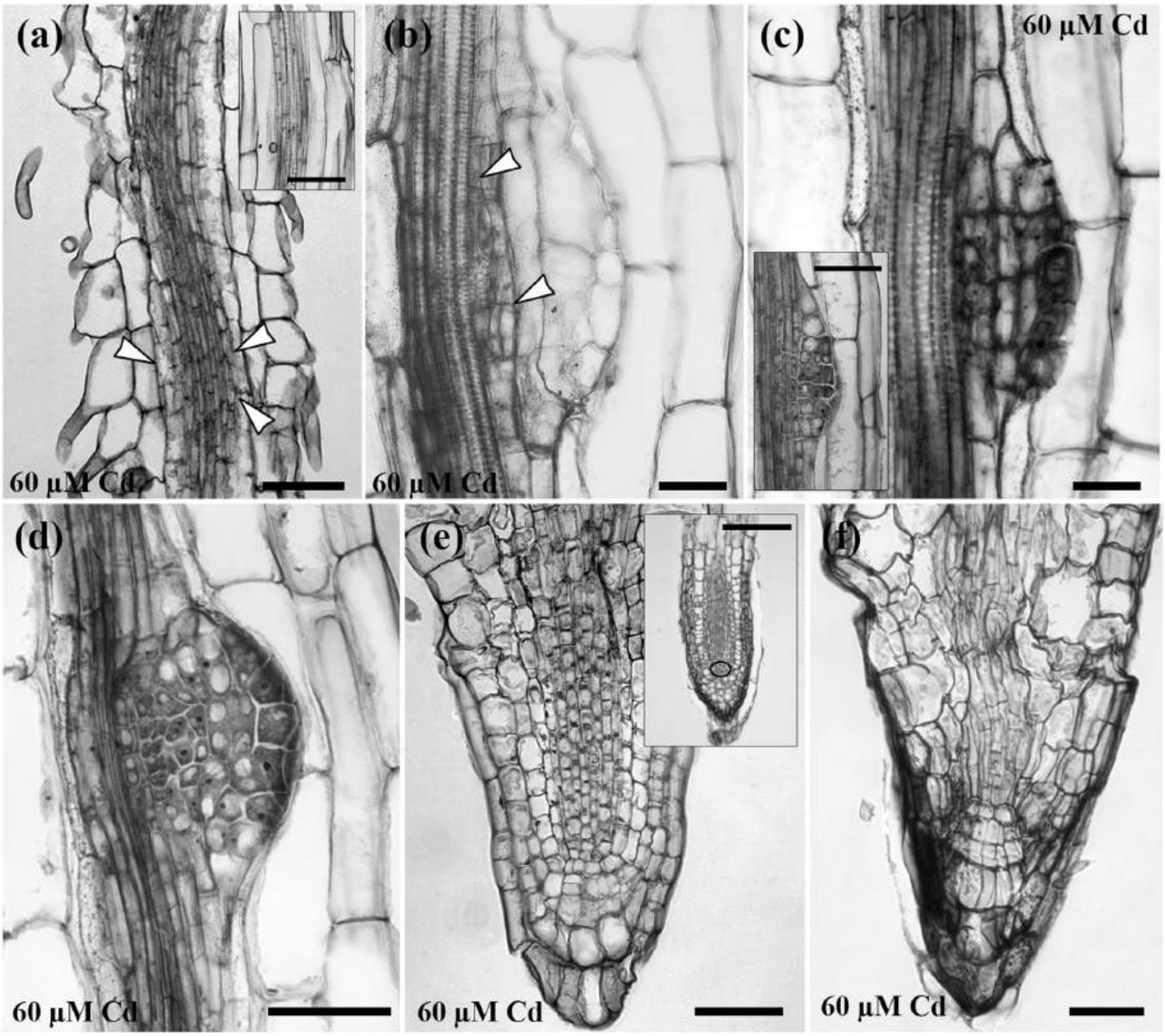

Fig. 7. Histological images of lateral root primordia (LRPs) at different developmental stages (a-d) and of lateral roots (LRs) (e,f) in 10-day-old *cat2–1* seedlings grown in the presence of 60 µM $CdSO_4$ (60 µM Cd). Main panels show *cat2–1* LRPs and LRs; insets show Col–0 LRPs and a LR at the same developmental stages. Insets show a PR (a), a LRP (c) and a LR (e) of Col–0 seedlings grown in the presence of 60 µM Cd. Images are representative of three biological replicates. Arrowheads (a) and (b) indicate anomalous cell divisions. Black circle in the inset in (e) marks the quiescent centre cells. Bars = 25 µm (b,c); 50 µm (a, inset in a, inset in c,d-f); 100 µm (inset in e).

Overall, these results indicate that the absence of CAT2 is associated with enhanced $^{\bullet}$NO-related signal in the PR, without major changes in the spatial distribution of either RNS analysed. Cadmium exposure increased •NO- and $ONOO^-$-related signals in the PRs of both genotypes, although the APF fluorescence showed a broader spatial distribution in *cat2–1*. In contrast, RNS-related signals in LRPs remained largely unaffected by either genotype or Cd exposure, indicating a root-type-specific response.

3.6. *The cat2 mutation negatively affects LRP initiation and development and enhances Cd-induced cyto-histological damage*

Given the observed effects of the *cat2* mutation on the development of the PR and LRPs, as well as on the accumulation and distribution of RNS and specifically on the ROS-related signals within these roots, a detailed cyto-histological analysis of Col–0 and *cat2–1* PRs, either exposed or not exposed to Cd, was conducted, particularly during the early stages of LRP formation. In *cat2–1* PRs, not exposed to Cd, a consistent and anomalous increase in pericycle cell proliferation was observed (Fig. 6a, arrowheads) compared to wild-type (Fig. 6a, inset). Notably, in *cat2–1,* the first divisions in LRP-founder cells of the pericycle were mainly periclinal (Fig. 6b, arrowhead), in contrast to the canonical anticlinal pattern of Arabidopsis LRP initiation (Fig. 6b, inset) (Malamy and Benfey, 1997). As a result, overlapping layers of irregular, newly formed cells were recurrently produced (Fig. 6c,d) instead of the two distinct layers needed for proper LRP formation as, in fact, seen in the wild-type (Fig. 6c, inset; Fig. 6d, inset). As a consequence, *cat2–1* LRPs failed to establish a well-defined meristematic dome, resulting in irregular structures (Fig. 6e–g). These altered domes were characterised by the random presence of prematurely differentiated cells, identifiable by large vacuoles (Fig. 6d, arrowhead; Fig. 6h, arrowhead), and by anomalous cell division planes (Fig. 6g, arrowheads). Moreover, these

irregular domes failed to specify a proper protoderm or to establish a correct quiescent centre (QC) (Fig. 6g–h), in contrast to what observed in Col−0 (Fig. 6h, inset and Fig. 6i). These defects persisted in the few LRPs that developed into LRs, which showed altered strands of procambial cells and irregular division activity in the protoderm and subtending layer (Fig. 6i).

In *cat2–1*, Cd exposure further exacerbated these cyto-histological alterations (Fig. 7). In particular, enhanced proliferation of the PR vascular parenchyma and abnormal pericycle activity were observed (Fig. 7a, arrowheads), together with numerous periclinal divisions in the pericycle cells (Fig. 7b, arrowheads), which generated overlapping cell layers (Fig. 7b), resulting in highly distorted LRP structures (Fig. 7c). These malformed domes consisted of differentiated cells that were unable to establish a functional root meristem. Similar alterations were observed in Cd-treated Col−0 roots, but they were generally less pronounced and less widespread (Fig. 7a, inset; Fig. 7c, inset). Although some LRPs developed a nearly regular dome shape, many of their cells were vacuolated and unable to establish a functional QC (Fig. 7d). Consequently, the few developing LRPs gave rise to highly anomalous LRs characterized by profound alterations at the root apex, including disorganization of the meristematic tissue architecture, cellular hypertrophy, precocious cellular differentiation, reduction of meristematic cells and, consequently, changes in meristem size, as well as loss of QC definition (Fig. 7e,f). In addition, in some cases, the apex consisted only of differentiated cells, which were hypertrophic and often underwent lysis (Fig. 7f). Even in Col−0 exposed to Cd, the elongated LRs showed histological alterations, with a partially disorganised root meristem but with a still detectable QC (Fig. 7e, inset).

Overall, the cyto-histological analysis reveals that the absence of CAT2 leads to pronounced alterations in LRP formation, including altered division-plane orientation in founder pericycle cells, premature cell differentiation, disorganised meristematic domes, and the absence of a clearly identifiable QC. Cadmium exposure further amplifies these defects, highlighting the combined impact of CAT2 deficiency and the metal stress in affecting root developmental plasticity.

4. Discussion

In this study, using *Arabidopsis thaliana cat2–1*, a mutant line lacking the *CAT2* gene encoding the isozyme responsible for the main CAT activity (Bueso et al., 2007), we uncover a direct involvement of the CAT2 protein in the development of the Arabidopsis root system, both in the absence and presence of Cd-induced stress. Specifically, the lack of CAT2 alters phytohormone and phenolic compound homeostasis and affects the development of the PR and of post-embryonic-derived LRs by modifying ROS and RNS distribution and accumulation in root tissues, with most of these alterations being further exacerbated under Cd exposure. Interestingly, most of the alterations observed in *cat2–1* roots under Control conditions resembled those induced by Cd treatment in wild-type seedlings, particularly with respect to ROS accumulation. This further supports the role of CAT2 in sustaining root system development through the maintenance of redox homeostasis. Indeed, in the root meristem, ROS accumulate differentially along the proliferation-to-differentiation axis, establishing redox gradients that regulate cell cycle progression, meristem maintenance, and cell differentiation (Tsukagoshi et al., 2010). Therefore, impaired CAT2-dependent ROS scavenging may disturb these spatial redox cues, thereby contributing to the altered cell division and differentiation patterns observed in *cat2–1* roots. In addition, our data reveal a differential response of LRs and the PR, with the mutation exerting stronger effects on LR formation and development. This supports a direct role for CAT2 in Arabidopsis root system development, beyond its involvement in stress-response regulation.

4.1. CAT2 protein is present at substantial levels in the Arabidopsis root system and increases in response to Cd

Using immunodetection analyses, we showed that CAT2 is present at appreciable levels within the Arabidopsis root system (Fig. 1). The marked reduction in the total CAT immunoreactive signal observed in *cat2–1* roots, which lack CAT2, suggests that CAT2 may represent a major contributor to the overall catalase pool in this organ, although the contributions of CAT1 and CAT3 cannot be determined from the present analysis. This interpretation is consistent with the decrease in total CAT activity reported in Arabidopsis roots following the loss of CAT2, but not CAT1 or CAT3, function (Yang et al., 2019).

Most studies addressing the role of CAT in plant responses to environmental stresses, including heavy metal exposure (Leung, 2018; Raza et al., 2025), have primarily focused on aerial organs or on the whole plant, without considering the specific contribution of CAT to root system development. Because total CAT levels are substantially higher in leaves than in roots (Chioti and Zervoudakis, 2017), as also confirmed in this study (Fig. 1; Supplementary Fig. 3), whole-plant analyses may mask root-specific responses and thereby underestimate the role of these proteins in root development under physiological conditions as well as in stress adaptation. Here, we show that Cd treatment slightly increases the total CAT protein pool in roots, suggesting increased CAT protein accumulation in response to heavy metal stress. However, this may not directly translate into increased enzymatic activity, as enzyme activity is regulated by multiple factors, including post-translational modifications and the cellular redox environment. By contrast, *Glycine max* plants exposed to 200 μM $CdCl_2$ showed a decline in total root CAT activity (Balestrasse et al., 2008), while *Triticum aestivum* seedlings exposed to arsenic for 48 h exhibited reduced expression of *CAT1*, *CAT2*, and *CAT3* genes in roots (Tyagi et al., 2021). However, in line with our results, *CAT* expression and enzyme activity in *Arundo donax* and *Agave sisalana* roots increased in response to Cd exposure (Santoro et al., 2022; Li et al., 2023). These discrepancies in CAT dynamics in roots highlight the importance of clarifying the role of CAT isozymes in root development under both stress and non-stress conditions. They also indicate that the type of pollutant, the nature and duration of the stress, the plant species, the root type, and the specific CAT isozyme should all be considered when evaluating the role of CAT in stress responses.

4.2. Phytohormone and phenolic compound homeostasis is altered by the lack of CAT2 in the root system

We demonstrate that the absence of CAT2, under physiological conditions, alters the content of key phytohormones and phenolic compounds in the root system (Fig. 3). Specifically, the *cat2–1* root system showed a significant increase in *trans*-zeatin *(tZ)*-type cytokinins, particularly *tZ* riboside (*tZR*), and in most phenolic compounds. In contrast, the levels phaseic acid, a major ABA catabolite, were decreased, whereas auxins and JAs levels remained unaffected. *tZR* is a major tZ-type cytokinin and may contribute to cytokinin activity after conversion to active forms, with important roles in plant performance under both normal and stress conditions (Frank et al., 2020; Zaheer et al., 2024). The elevated *tZR* levels observed in *cat2–1* roots may be associated with ROS-dependent changes in cytokinin metabolism, possibly involving cytokinin oxidase/dehydrogenase (CKX) enzymes, which catalyse the irreversible degradation of cytokinins with substrate-specific affinities and efficiencies (Cueno et al., 2012). In addition, isopentenyl adenine (iP) levels were similar in both genotypes and increased similarly in response to Cd. This indicates that these two major isoprenoid-type cytokinins, despite belonging to the same hormonal class, respond differently to CAT2 deficiency and Cd exposure, likely reflecting regulation through distinct biosynthetic and/or signalling pathways (Sakakibara, 2006). Jasmonates and CAT are known to interact in physiological processes occurring in aerial organs, including stomatal closure and leaf senescence (Jannat et al., 2012; Zhang et al.,

2020). However, CAT2 does not appear to affect the levels of bioactive JAs in leaves, since JA and JA-Ile levels in the wild-type and in *cat2–1* were essentially similar. In contrast, the mutant displays a marked accumulation of OPDA and of hydroxylated, glucosylated, and sulfated derivatives of JA and JA-Ile (Lelarge-Trouverie et al., 2023). Consistently, our results show that JA and JA-Ile levels are comparable in the root systems of wild-type and *cat2–1*, whereas higher levels of JA-derivatives, such as dihydrojasmonic acid, are detected in the mutant line. Together, these observations suggest that, under physiological conditions, the interaction between CAT2 and JA or JA-Ile does not lead to changes in bioactive JA, but rather to a reallocation of jasmonate metabolites.

In addition, Cd exposure did not increase root JA or JA-Ile levels in *cat2–1*, whereas both metabolites increased in the wild-type, suggesting that CAT2 contributes to jasmonate homeostasis under Cd stress. In line with this, under pathogen infection, CAT2 has been shown to actively promote JA production through its interaction with the JA-biosynthetic enzymes ACX2 and ACX3 in peroxisomes, and accordingly, *cat2–1* shows reduced JA levels (Yuan et al., 2017).

Surprisingly, the levels of the auxin IAA and of its biosynthetic precursor IAM were not significantly altered in *cat2–1* roots compared to the wild-type. This finding contrasts with previous reports of reduced IAA levels in Arabidopsis *cat2–1* plants (Gao et al., 2014; Yuan et al., 2017). This discrepancy is particularly noteworthy because *cat2–1* is characterised by enhanced photorespiratory H_2O_2 production, and photorespiration-derived H_2O_2 has been shown to influence auxin biosynthesis by modulating the expression of genes involved in Trp-dependent IAA biosynthesis and IBA-to-IAA conversion, at least in rice (Li et al., 2021).

The discrepancy between our results and previous reports obtained in Arabidopsis *cat2–1*, may be explained by several experimental differences. First, our analyses were specifically performed on roots, whereas previous studies focused on aerial tissues or whole-plant, suggesting that the relationship between photorespiratory H_2O_2 and auxin metabolism may be organ-specific. Second, photorespiration is a light-dependent process, and differences in light conditions between studies may have influenced the extent of H_2O_2 production and its downstream effects on auxin biosynthesis. Finally, our experiments were performed on 10-day-old seedlings, whereas previous studies used more mature plants, at a developmental stage where auxin metabolism may differ considerably.

Interestingly, Cd treatment affected IAA and IAM levels only in *cat2–1* roots, increasing their accumulation and suggesting a compensatory adjustment of auxin metabolism in the absence of CAT2. This highlights a possible role for CAT2 in the regulation of root auxin homeostasis in response to environmental pollutants, at least Cd, although the underlying mechanism remains to be fully characterised.

Finally, we found that *cat2–1* roots accumulate higher levels of phenolic compounds, particularly SAG, PAAM and ferulic acid. Regarding the possible roles of these phenolics, SAG, an inactive glucosylated form of SA, may contribute to buffering SA-dependent redox signalling, since SA is known to be a key regulator of redox responses that can also promote ROS overproduction (Saleem et al., 2021). Consistently, Lelarge-Trouverie et al. (2023) found increased levels of SA and its glucosylated form SAG in *cat2–1* leaves compared with the wild-type, interpreting this as part of a compensatory response to oxidative stress induced by the mutation. The increases in PAAM and ferulic acid may also contribute to limiting excessive ROS accumulation, given their antioxidant activity (Pattanashetty et al., 2018; Khan et al., 2024). However, Cd exposure reduced the levels of these compounds in *cat2–1* roots. In this regard, the decreased SAG accumulation might indicate the activation of SA-mediated stress responses, while the reduction in ferulic acid may result from impaired antioxidant metabolite accumulation caused by excessive ROS production.

4.3. CAT2 is involved in primary root elongation, lateral root formation, and in modulating root ROS- and RNS-related patterns

We showed that the *cat2–1* mutant exhibits reduced PR elongation, regardless of Cd application, starting from 10 days after sowing (Fig. 2). This finding is consistent with the results of Yang et al. (2019), who also reported reduced PR elongation in *cat2–1* under physiological conditions. According to these authors, the PR growth inhibition was alleviated or completely restored by the addition of sucrose to the growth medium or by elevated atmospheric CO_2, thus highlighting an important role of the photosynthetic and photorespiratory pathways of the aerial organs in affecting PR elongation (Yang et al., 2019). Conversely, we here show that PR elongation is reduced in *cat2–1*, despite the presence of sucrose in the growing medium, at concentrations comparable to those previously reported by the authors. Thus, it is possible that the arrest in PR elongation can be directly attributed to alterations in the root apex itself (i.e., the root part responsible for elongation), associated with mutation-induced redox imbalance, as suggested by our ROS and RNS analyses rather than to an indirect effect arising from the mutation-induced effects in aerial organs (Figs. 4, 5 and Supplementary Fig. 7).

Although a reduced PR elongation is often compensated by an increased LR production (Ingram et al., 2011), this was not the case for *cat2–1* under our growth conditions. Instead, we observed a decrease in LR formation. This is consistent with Bueso et al. (2007), who reported fewer LRs in Arabidopsis *cat2–1*, a phenotype that the authors attributed to the mutant's reduced sensitivity to ethylene, a known positive regulator of LR development via NAC2.

Additionally, the same reduced LR production observed in the *cat2/3* double mutant was linked to a reduced sensitivity to IBA, an auxin widely known to induce LR. This effect was attributed to impaired peroxisomal β-oxidation caused by the mutation, which may affect IBA-to-IAA conversion (Schlicht et al., 2013; Su et al., 2018).

Consistent with these observations, our metabolomic analysis (Fig. 3) revealed a trend toward lower accumulation of IAA and several of its conjugated derivatives, including IAA-Asp, IAA-Glu, and IAA-GE, in *cat2–1* roots under Control conditions. Given the central role of auxin accumulation in pericycle cells as an instructive trigger for their re-specify into lateral root founder cells (Dubrovsky et al., 2008), and the critical role of local auxin maximum definition in the nascent LRPs (Péret et al., 2009; Fattorini et al., 2017) even a subtle reduction in auxin availability could underlie the impaired LR formation observed in *cat2–1*. Auxin-responsive reporters such as DR5 in *cat2–1* background could be used in future studies to further refine the spatial interpretation of this response at the tissue level.

Our cyto-histological analysis shows that LR defects in *cat2–1* result from altered cell division activity in the pericycle, the tissue typically responsible for LR formation, as well as from abnormal patterns of cell differentiation and division in the root meristem (Figs. 6 and 7). Consequently, many LRPs fail to develop into mature LRs. Our histochemical and confocal microscopy analyses suggest that the alterations observed during the early stages of LRP development, both in primordium cell division-plane orientation and in the proliferation of the competent tissues, arise from changes in the accumulation and spatial distribution of root RNS and, in particular, of ROS, with possible consequences at the cytoskeletal level (Figs. 4 and 5). Indeed, changes in root ROS accumulation are known to profoundly alter the organisation of the tubulin cytoskeleton during interphase, preprophase, and the different stages of the mitotic cycle and phragmoplast formation, thereby having a substantial impact on the proper progression of cell division in this organ (Livanos et al., 2012, 2017). Consistent with this, Arabidopsis lines with induced microtubule depolymerisation exhibit an altered LRP morphology (Stöckle et al., 2022), closely resembling that observed here in *cat2–1*.

Furthermore, the altered LR development observed in *cat2–1* may also be related to a mutation-induced disruption of ROS gradients within

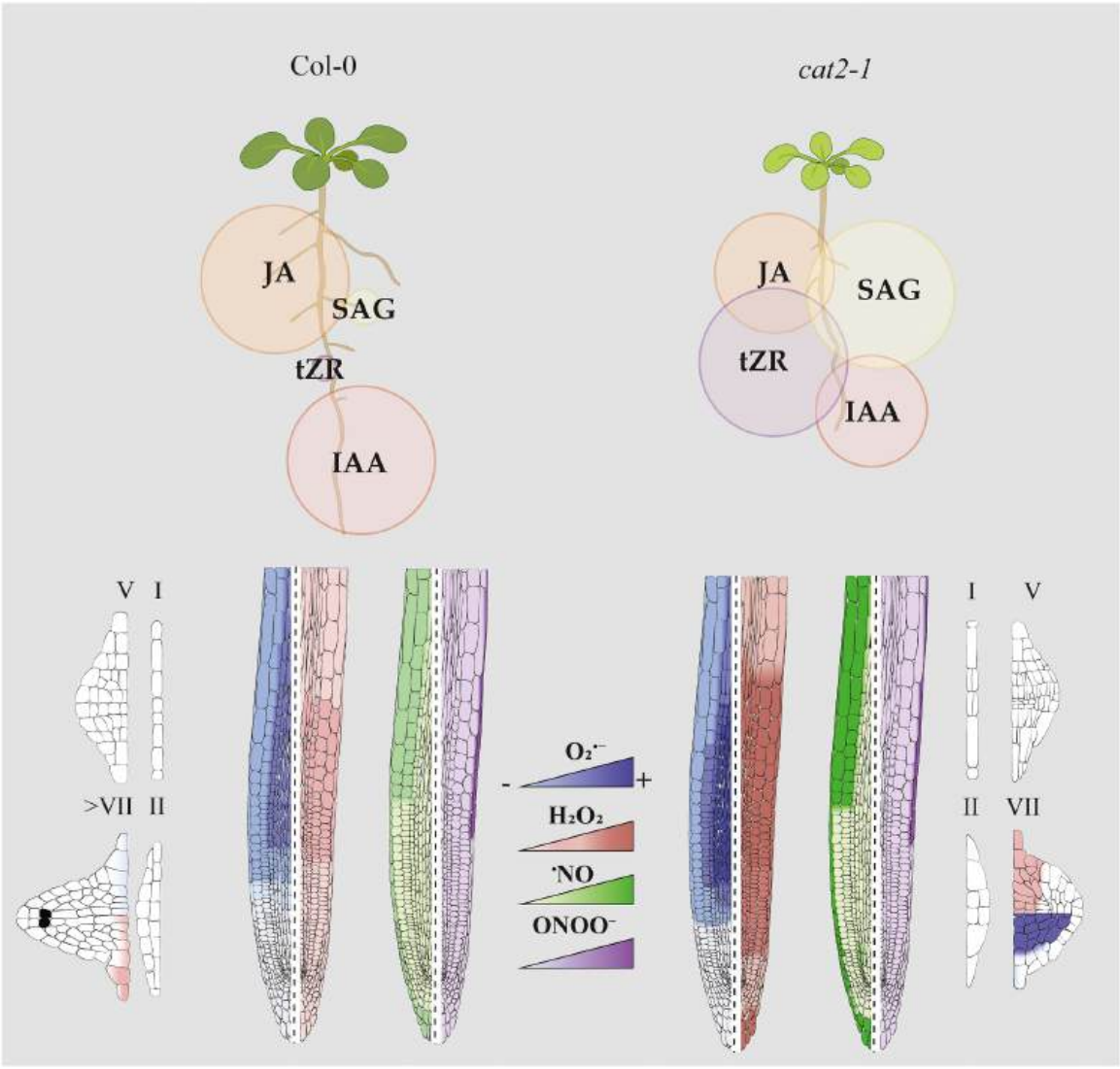

Fig. 8. Representative illustration highlighting the main differences between wild-type (Col−0, left) and *cat2−1* mutant (right) in root morphology, metabolite content, ROS/RNS accumulation/distribution, and LR development in 10-day-old *Arabidopsis thaliana* seedlings grown under Control conditions. Compared with Col−0, *cat2−1* displays a shorter PR, reduced LR formation, and altered levels of key metabolites, including jasmonates (JA, orange bubble), phenolics (SAG, yellow bubble), cytokinins (tZR, purple bubble), and auxins (IAA, red bubble) (top right). Differences in metabolite content between *cat2−1* and Col−0 are represented proportionally by bubble size. *cat2−1* shows altered LRP development due to defects in founder cell division and altered differentiation patterns, leading to morphological abnormalities and developmental arrest (bottom right). The figure schematically depicts these alterations at stages I, II, V, and VII of LRP development according to Malamy and Benfey (1997). In Col−0, LRP development proceeds normally beyond stage VII, with the establishment of the quiescent centre occurs (black cells) (bottom left). *cat2−1* displays altered accumulation and distribution of major ROS and RNS within the root cells, in the PR tips and in stage VII LRPs. The distribution of each reactive species is indicated by distinct colours: blue for superoxide ($O_2^{\bullet-}$), pink for hydrogen peroxide (H_2O_2), green for nitric oxide (NO), and violet for peroxynitrite ($ONOO^-$). Differences observed between Col−0 and *cat2−1* under Cd treatment are discussed in the main text. IAA = indole−3-acetic acid; JA = jasmonic acid; LR = lateral root; LRP = lateral root primordium; PR = primary root; ROS = reactive oxygen species; RNS = reactive nitrogen species; SAG = salicylic acid glucoside; *t*ZR = trans-zeatin riboside.

the developing primordium itself. As previously discussed, disruption of the ROS gradient along the root meristem–elongation–differentiation axis in Arabidopsis can compromise both the maintenance of the root stem cell niche and proper organ differentiation. In this context, CAT2, together with UPB1-mediated redox regulation, may contribute to preserving the spatial redox balance required for normal root development (Tsukagoshi et al., 2010). Supporting this hypothesis, we demonstrate that the *cat2–1* roots display an enhanced accumulation and altered spatial distribution of ROS, particularly of H_2O_2 and $O_2^{\bullet-}$-related signals, especially in the PR meristems and in the tissues undergoing LRP development (Fig. 4). The increased H_2O_2 signal observed in *cat2–1* roots is consistent with the absence of the CAT2 isozyme and supports its prominent contribution in H_2O_2 scavenging in the root tissues under physiological pathways generating H_2O_2, such as peroxisomal fatty acid β-oxidation. In accordance, *CAT2* mRNA abundance in Arabidopsis roots is higher than that of the other catalase isozymes, with a peak of expression at the root apex (Brady et al., 2007).

Moreover, the altered $O_2^{\bullet-}$ signal in *cat2–1* roots can be attributed to changes in peroxisome functionality caused by the mutation. Indeed, it is known that CAT2, which contains a peroxisomal targeting signal (PTS1), predominantly accumulates within peroxisomes, and that Arabidopsis seedlings mutated in this isozyme exhibit peroxisomal aggregation and oxidation, followed by autophagy (Shibata et al., 2013). As peroxisomes are recognised as a key site of $O_2^{\bullet-}$ metabolism (Corpas et al., 2020), it is likely that the *cat2* mutation, by altering the function of these organelles, contributes to the disruption in accumulation

and distribution patterns of this ROS in the root system. This effect may be particularly pronounced in the root apical meristems, where peroxisomes are abundant, and the peroxisome-to-cytoplasm ratio is high, as reported in the root meristem of *Allium cepa* (Collings et al., 2003) and Arabidopsis PRs and LRs, possibly reflecting a cyto-protective mechanism (Piacentini et al., 2020). The same altered peroxisomal involvement might explain the enhanced •NO-signal observed in *cat2–1* PRs, as •NO, like $O_2^{\bullet -}$, is tightly regulated also at the peroxisomal level (Fig. 5) (Corpas et al., 2022).

Cadmium treatment was here demonstrated to enhance all the analysed ROS and RNS in the root, particularly in the apical meristem. This observation confirms the root apical meristem as a primary target of the pollutant's toxicity, with a strong impact on the redox-related cellular processes, in turn supporting variations in ROS and RNS molecules as key indicators of the plant response to Cd stress (Yuan and Huang, 2016; Romero-Puertas et al., 2019; Talarico et al., 2025).

Compared to the wild-type, *cat2–1* roots displayed stronger Cd-induced ROS accumulation and spatial distribution, whereas RNS-related signals were affected, but at a lower level than in Col−0. This finding supports a specific contribution of CAT2 to ROS detoxification under Cd exposure, also suggesting that excess in RNS may be scavenged through CAT2-independent pathways. Nevertheless, it has been recently demonstrated that, under physiological conditions, CAT and RNS interact through RNS-derived post-translational modifications (PTMs), including $ONOO^-$-mediated nitration and •NO-dependent S-nitrosation, which can downregulate CAT activity and promote H_2O_2 accumulation (Corpas et al., 2009; Corpas and Barroso, 2014; González-Gordo et al., 2024). Therefore, further analyses are needed to elucidate the interplay between CAT2 and RNS in the root system of Arabidopsis, as well as of other species.

Overall, our results suggest that mutation-dependent alterations in redox-related signals are closely associated with changes in root system development, whereas the CAT-mediated redox response to Cd is ROS/RNS specific. However, the observation that the *cat2* mutation negatively affects LRP initiation and development, together with the finding that some alterations observed under Control conditions resemble those induced by Cd treatment in wild-type roots, suggest that CAT2 may have an important morphogenic role in the formation of LR that is stress-independent, although the mechanisms underlying this resemblance remain to be fully elucidated.

5. Conclusions

In conclusion, our results support a key role of Arabidopsis CAT2 in root system development, particularly to primary root elongation and in the formation and development of lateral root primordia, opening new avenues for future investigation. This function is likely linked to CAT2-dependent modulation of hormonal homeostasis, the accumulation of secondary metabolites with antioxidant functions, and the accumulation and spatial distribution of ROS and RNS within the root system, as schematically illustrated in Fig. 8. These processes appears particularly important for cell division and differentiation within root tissues and might explain some of the effects linking organ plasticity to stress response.

CRediT authorship contribution statement

Marta Rodríguez-Ruiz: Investigation, Data curation. **Donato De Girolamo:** Investigation, Data curation. **Federica Della Rovere:** Investigation, Data curation. **Corpas Francisco Javier:** Investigation, Data curation. **Giuseppina Falasca:** Writing – review & editing. **Alice Peduzzi:** Investigation, Data curation. **D'Angeli Simone:** Investigation, Data curation. **Barbora Svobodová:** Investigation, Data curation. **Maria Maddalena Altamura:** Writing – review & editing. **Diego Piacentini:** Writing – review & editing, Writing – original draft, Validation, Methodology, Investigation, Formal analysis, Data curation, Conceptualization. **Petre Dobrev:** Investigation, Data curation. **Matteo Fedeli:** Investigation, Data curation. **Giulia Calonzi:** Investigation, Data curation.

Funding

This study was financially supported by Sapienza Università di Roma (grant numbers RM1221815D29A543 to DP and RM124190DAE1BF7D to GF). Francisco J. Corpas' research is supported by the European Regional Development Fund co-financed grants from the Ministry of Science and Innovation (PID2023-146153NB-C21), Spain. The confocal microscope used for this study was purchased with funds from the "Dipartimento di Eccellenza MUR 2023–2027" program.

Declaration of Competing Interest

The authors declare that they have no known competing financial interests or personal relationships that could have appeared to influence the work reported in this paper.

Acknowledgements

The authors thank Dr Valentina Cecchetti for her valuable assistance with the PCR-based validation of the *cat2–1* line. This study was financially supported by Sapienza Università di Roma (grants numbers RM1221815D29A543 to DP and RM124190DAE1BF7D to GF). Francisco J Corpas research is supported by the European Regional Development Fund co-financed grants from the Ministry of Science and Innovation (PID2023-146153NB-C21), Spain. The confocal microscope used for this study was purchased with funds from the "Dipartimento di Eccellenza MUR 2023–2027" program.

Appendix A. Supporting information

Supplementary data associated with this article can be found in the online version at doi:10.1016/j.envexpbot.2026.106406.

Data availability

The data supporting the findings of this study are available from the corresponding author upon reasonable request.

References

Alonso, J.M., Stepanova, A.N., Leisse, T.J., Kim, C.J., Chen, H., Shinn, P., Ecker, J.R., 2003. Genome-wide insertional mutagenesis of *Arabidopsis thaliana*. Science 301, 653–657. https://doi.org/10.1126/science.1086391.

Altamura, M.M., Piacentini, D., Della Rovere, F., Fattorini, L., Falasca, G., Betti, C., 2023. New paradigms in brassinosteroids, strigolactones, sphingolipids, and nitric oxide interaction in the control of lateral and adventitious root formation. Plants 12, 413. https://doi.org/10.3390/plants12020413.

Baker, A., Lin, C.C., Lett, C., Karpinska, B., Wright, M.H., Foyer, C.H., 2023. Catalase: a critical node in the regulation of cell fate. Free. Radic. Biol. Med. 199, 56–66. https://doi.org/10.1016/j.freeradbiomed.2023.02.009.

Balestrasse, K.B., Yannarelli, G.G., Noriega, G.O., Batlle, A., Tomaro, M.L., 2008. Heme oxygenase and catalase gene expression in nodules and roots of soybean plants subjected to cadmium stress. Biometals 21, 433–441. https://doi.org/10.1007/s10534-008-9132-0.

Brady, S.M., Orlando, D.A., Lee, J.Y., Wang, J.Y., Koch, J., Dinneny, J.R., Mace, D., Ohler, U., Benfey, P.N., 2007. A high-resolution root spatiotemporal map reveals dominant expression patterns. Science 318, 801–806. https://doi.org/10.1126/science.1146265.

Bueso, E., Alejandro, S., Carbonell, P., Perez-Amador, M.A., Fayos, J., Bellés, J.M., Rodriguez, P.L., Serrano, R., 2007. The lithium tolerance of the *Arabidopsis cat2* mutant reveals a cross-talk between oxidative stress and ethylene. Plant. J. 52, 1052–1065. https://doi.org/10.1111/j.1365-313X.2007.03305.x.

Chioti, V., Zervoudakis, G., 2017. Is root catalase a bifunctional catalase-peroxidase? Antioxidants 6, 39. https://doi.org/10.3390/antiox6020039.

Collings, D.A., Harper, J.D., Vaughn, K.C., 2003. The association of peroxisomes with the developing cell plate in dividing onion root cells depends on actin microfilaments and myosin. Planta 218, 204–216. https://doi.org/10.1007/s00425-003-1096-2.

Corpas, F.J., 2016. Reactive nitrogen species (RNS) in plants under physiological and adverse environmental conditions: current view. Progress. Bot. 78, 97–119.
Corpas, F.J., Barroso, J.B., 2014. Peroxynitrite ($ONOO^-$) is endogenously produced in arabidopsis peroxisomes and is overproduced under cadmium stress. Ann. Bot. 113, 87–96. https://doi.org/10.1093/aob/mct260.
Corpas, F.J., Hayashi, M., Mano, S., Nishimura, M., Barroso, J.B., 2009. Peroxisomes are required for in vivo nitric oxide accumulation in the cytosol following salinity stress of *Arabidopsis* plants. Plant. Physiol. 151, 2083–2094. https://doi.org/10.1104/pp.109.146100.
Corpas, F.J., González-Gordo, S., Palma, J.M., 2020. Plant peroxisomes: a factory of reactive species. Front. Plant. Sci. 11, 551823. https://doi.org/10.3389/fpls.2020.00853.
Corpas, F.J., González-Gordo, S., Palma, J.M., 2022. NO source in higher plants: present and future of an unresolved question. Trends Plant. Sci. 27, 116–119. https://doi.org/10.1016/j.tplants.2021.11.016.
Corpas, F.J., González-Gordo, S., Muñoz-Vargas, M.A., Rodríguez-Ruiz, M., Ruiz-Torres, C., Palma, J.M., 2025. Endogenous NO fluctuations in *Arabidopsis* leaves influence peroxisomal activities and ROS, NADPH, and H_2S metabolism. Plant. Sci. 359, 112683. https://doi.org/10.1016/j.plantsci.2025.112683.
Cueno, M.E., Imai, K., Ochiai, K., Okamoto, T., 2012. Cytokinin dehydrogenase differentially regulates cytokinin and indirectly affects hydrogen peroxide accumulation in tomato leaf. J. Plant. Physiol. 169, 834–838. https://doi.org/10.1016/j.jplph.2012.01.008.
Dai, L., Li, J., Harmens, H., Zheng, X., Zhang, C., 2020. Melatonin enhances drought resistance by regulating leaf stomatal behaviour, root growth, and catalase activity in two contrasting rapeseed *(Brassica napus* L.) genotypes. Plant. Physiol. Biochem. 149, 86–95. https://doi.org/10.1016/j.plaphy.2020.01.039.
Della Rovere, F., Piacentini, D., Fattorini, L., Girardi, N., Bellanima, D., Falasca, G., Altamura, M.M., Betti, C., 2022. Brassinosteroids mitigate cadmium effects in *Arabidopsis* root system without any cooperation with nitric oxide. Int. J. Mol. Sci. 23, 825. https://doi.org/10.3390/ijms23020825.
Dubrovsky, J.G., Sauer, M., Napsucialy-Mendivil, S., Ivanchenko, M.G., Friml, J., Shishkova, S., Celenza, J., Benková, E., 2008. Auxin acts as a local morphogenetic trigger to specify lateral root founder cells. Proc. Natl. Acad. Sci. 105, 8790–8794. https://doi.org/10.1073/pnas.0712307105.
Fattorini, L., Ronzan, M., Piacentini, D., Della Rovere, F., De Virgilio, C., Sofo, A., Altamura, M.M., Falasca, G., 2017. Cadmium and arsenic affect quiescent centre formation and maintenance in *Arabidopsis thaliana* post-embryonic roots disrupting auxin biosynthesis and transport. Environ. Exp. Bot. 144, 37–48. https://doi.org/10.1016/j.envexpbot.2017.10.005.
Frank, M., Cortleven, A., Novák, O., Schmülling, T., 2020. Root-derived trans-zeatin cytokinin protects *Arabidopsis* plants against photoperiod stress. Plant. Cell. Environ. 43, 2637–2649. https://doi.org/10.1111/pce.13860.
Frugoli, J.A., Zhong, H.H., Nuccio, M.L., McCourt, P., McPeek, M.A., Thomas, T.L., McClung, C.R., 1996. Catalase is encoded by a multigene family in *Arabidopsis thaliana* (L.) Heynh. Plant. Physiol. 12, 327–336. https://doi.org/10.1104/pp.112.1.327.
Gallego, S.M., Benavides, M.P., 2019. Cadmium-induced oxidative and nitrosative stress in plants. In: Hasanuzzaman, M., Narasimha, M., Prasad, V., Fujita, M. (Eds.), Cadmium toxicity and tolerance in plants. Academic Press, London, UK, pp. 233–274. https://doi.org/10.1016/B978-0-12-814864-8.00010-3.
Gao, X., Yuan, H.M., Hu, Y.Q., Li, J., Lu, Y.T., 2014. Mutation of Arabidopsis CATALASE2 results in hyponastic leaves by changes of auxin levels. Plant. Cell. Environ. 37, 175–188. https://doi.org/10.1111/pce.12144.
González-Gordo, S., López-Jaramillo, J., Rodríguez-Ruiz, M., Taboada, J., Palma, J.M., Corpas, F.J., 2024. Pepper catalase: a broad analysis of its modulation during fruit ripening and by nitric oxide. Biochem. J. 481, 883–901. https://doi.org/10.1042/BCJ20240247.
Guan, Z., Chai, T., Zhang, Y., Xu, J., Wei, W., 2009. Enhancement of Cd tolerance in transgenic tobacco plants overexpressing a Cd-induced catalase cDNA. Chemosphere 76, 623–630. https://doi.org/10.1016/j.chemosphere.2009.04.047.
Hernandez, M., Fernandez-Garcia, N., Diaz-Vivancos, P., Olmos, E., 2010. A different role for hydrogen peroxide and the antioxidative system under short and long salt stress in *Brassica oleracea* roots. J. Exp. Bot. 61, 521–535.
Ingram, P., Dettmer, J., Helariutta, Y., Malamy, J.E., 2011. Arabidopsis Lateral Root Development 3 is essential for early phloem development and function, and hence for normal root system development. Plant. J. 68, 455–467. https://doi.org/10.1111/j.1365-313X.2011.04700.x.
Jannat, R., Uraji, M., Hossain, M.A., Islam, M.M., Nakamura, Y., Mori, I.C., Murata, Y., 2012. Catalases negatively regulate methyl jasmonate signaling in guard cells. J. Plant. Physiol. 169, 1012–1016. https://doi.org/10.1016/j.jplph.2012.03.006.
Kamada, T., Nito, K., Hayashi, H., Mano, S., Hayashi, M., Nishimura, M., 2003. Functional differentiation of peroxisomes revealed by expression profiles of peroxisomal genes in Arabidopsis thaliana. Plant. Cell. Physiol. 44, 1275–1289. https://doi.org/10.1093/pcp/pcg173.
Khan, K.A., Saleem, M.H., Afzal, S., Hussain, I., Ameen, F., Fahad, S., 2024. Ferulic acid: therapeutic potential due to its antioxidant properties, role in plant growth, and stress tolerance. Plant. Growth Regul. 104, 1329–1353. https://doi.org/10.1007/s10725-024-01243-w.
Lelarge-Trouverie, C., Cohen, M., Trémulot, L., Van Breusegem, F., Mhamdi, A., Noctor, G., 2023. Metabolite modification in oxidative stress responses: a case study of two defense hormones. Free. Radic. Biol. Med. 196, 145–155. https://doi.org/10.1016/j.freeradbiomed.2023.01.007.
Leung, D.W., 2018. Studies of catalase in plants under abiotic stress. In: Gupta, D.K., Palma, J.M., Corpas, F.J. (Eds.), Antioxidants and antioxidant enzymes in higher plants. Springer International Publishing, Cham, CH, pp. 27–39. https://doi.org/10.1007/978-3-319-75088-0_2.
Li, J., Ge, L., Liu, P., Huang, Z., Tan, S., Wu, W., Chen, T., Xi, J., Huang, X., Yi, K., 2023. Exploring cadmium stress responses in sisal roots: Insights from biochemical and transcriptome analysis. PLoS. One 18, e0288476. https://doi.org/10.1371/journal.pone.0288476.
Li, X., Liao, M., Huang, J., Xu, Z., Lin, Z., Ye, N., Zhang, Z., Peng, X., 2021. Glycolate oxidase-dependent H2O2 production regulates IAA biosynthesis in rice. BMC Plant. Biol. 21, 326. https://doi.org/10.1186/s12870-021-03112-4.
Liu, W.C., Han, T.T., Yuan, H.M., Yu, Z.D., Zhang, L.Y., Zhang, B.L., Zhai, S., Zheng, S.Q., Lu, Y.T., 2017. CATALASE2 functions for seedling postgerminative growth by scavenging H_2O_2 and stimulating ACX2/3 activity in *Arabidopsis*. Plant. Cell. Environ. 40, 2720–2728. https://doi.org/10.1111/pce.13031.
Livanos, P., Galatis, B., Quader, H., Apostolakos, P., 2012. Disturbance of reactive oxygen species homeostasis induces atypical tubulin polymer formation and affects mitosis in root-tip cells of *Triticum turgidum* and *Arabidopsis thaliana*. Cytoskeleton 69, 1–21. https://doi.org/10.1002/cm.20538.
Livanos, P., Galatis, B., Quader, H., Apostolakos, P., 2017. ROS homeostasis as a prerequisite for the accomplishment of plant cytokinesis. Protoplasma 254, 569–586. https://doi.org/10.1007/s00709-016-0976-9.
Malamy, J.E., 2005. Intrinsic and environmental response pathways that regulate root system architecture. Plant. Cell. Environ. 28, 67–77. https://doi.org/10.1111/j.1365-3040.2005.01306.x.
Malamy, J.E., Benfey, P.N., 1997. Organization and cell differentiation in lateral roots of *Arabidopsis thaliana*. Development 124, 33–44. https://doi.org/10.1242/dev.124.1.33.
Mhamdi, A., Queval, G., Chaouch, S., Vanderauwera, S., Van Breusegem, F., Noctor, G., 2010. Catalase function in plants: a focus on *Arabidopsis* mutants as stress-mimic models. J. Exp. Bot. 61, 4197–4220. https://doi.org/10.1093/jxb/erq282.
Murashige, T., Skoog, F., 1962. A revised medium for rapid growth and bio assays with tobacco tissue cultures. Physiol. Plant. 15, 473–497. https://doi.org/10.1111/j.1399-3054.1962.tb08052.x.
Ni, W., Trelease, R.N., 1991. Post-transcriptional regulation of catalase isozyme expression in cotton seeds. Plant. Cell. 3, 737–744. https://doi.org/10.1105/tpc.3.7.737.
Ono, M., Isono, K., Sakata, Y., Taji, T., 2021. CATALASE2 plays a crucial role in long-term heat tolerance of *Arabidopsis thaliana*. Biochem. Biophys. Res. Commun. 534, 747–751. https://doi.org/10.1016/j.bbrc.2020.11.006.
Péret, B., Larrieu, A., Bennett, M.J., 2009. Lateral root emergence: a difficult birth. J. Exp. Bot. 60, 3637–3643. https://doi.org/10.1093/jxb/erp232.
Palma, J.M., Mateos, R.M., López-Jaramillo, J., Rodríguez-Ruiz, M., González-Gordo, S., Lechuga-Sancho, A.M., Corpas, F.J., 2020. Plant catalases as NO and H_2S targets. Redox Biol. 34, 101525. https://doi.org/10.1016/j.redox.2020.101525.
Pattanashetty, S.H., Hosamani, K.M., Shettar, A.K., Mohammed Shafeeulla, R., 2018. Design, synthesis and computational studies of novel carbazole n-phenylacetamide hybrids as potent antibacterial, anti-inflammatory, and antioxidant agents. J. Heterocycl. Chem. 55, 1765–1774. https://doi.org/10.1002/jhet.3214.
Piacentini, D., Della Rovere, F., Sofo, A., Fattorini, L., Falasca, G., Altamura, M.M., 2020. Nitric oxide cooperates with auxin to mitigate the alterations in the root system caused by cadmium and arsenic. Front. Plant. Sci. 11, 1182. https://doi.org/10.3389/fpls.2020.01182.
Piacentini, D., Della Rovere, F., Bertoldi, I., Massimi, L., Sofo, A., Altamura, M.M., Falasca, G., 2021. Peroxisomal PEX7 receptor affects cadmium-induced ROS and auxin homeostasis in *Arabidopsis* root system. Antioxidants 10, 1494. https://doi.org/10.3390/antiox10091494.
Queval, G., Issakidis-Bourguet, E., Hoeberichts, F.A., Vandorpe, M., Gakière, B., Vanacker, H., Miginiac-Maslow, M., Van Breusegem, F., Noctor, G., 2007. Conditional oxidative stress responses in the *Arabidopsis* photorespiratory mutant *cat2* demonstrate that redox state is a key modulator of daylength-dependent gene expression, and define photoperiod as a crucial factor in the regulation of H_2O_2-induced cell death. Plant. J. 52, 640–657. https://doi.org/10.1111/j.1365-313X.2007.03263.x.
Raza, A., Bhardwaj, S., Anas, M., Su, W., Abbas, S., Li, Y., Guo, C., Corpas, F.J., Hu, Z., 2025. Role of plant peroxisomal catalase in temperature and drought stress: physio-biochemical and molecular perspectives. Plant. Physiol. Biochem. 229, 110730. https://doi.org/10.1016/j.plaphy.2025.110730.
Romero-Puertas, M.C., Terrón-Camero, L.C., Pelaez-Vico, M.A., Olmedilla, A., Sandalio, L.M., 2019. Reactive oxygen and nitrogen species as key indicators of plant responses to Cd stress. Environ. Exp. Bot. 161, 107–119. https://doi.org/10.1016/j.envexpbot.2018.10.012.
Sakakibara, H., 2006. Cytokinins: activity, biosynthesis, and translocation. Annu. Rev. Plant. Biol. 57, 431–449. https://doi.org/10.1146/annurev.arplant.57.032905.105231.
Saleem, M., Fariduddin, Q., Castroverde, C.D.M., 2021. Salicylic acid: a key regulator of redox signalling and plant immunity. Plant. Physiol. Biochem. 168, 381–397. https://doi.org/10.1016/j.plaphy.2021.10.011.
Santoro, D.F., Sicilia, A., Testa, G., Cosentino, S.L., Lo Piero, A.R., 2022. Global leaf and root transcriptome in response to cadmium reveals tolerance mechanisms in *Arundo donax* L. BMC Genom. 23, 427. https://doi.org/10.1186/s12864-022-08605-6.
Schlicht, M., Ludwig-Müller, J., Burbach, C., Volkmann, D., Baluska, F., 2013. Indole-3-butyric acid induces lateral root formation via peroxisome-derived indole-3-acetic acid and nitric oxide. New. Phytol. 200, 473–482. https://doi.org/10.1111/nph.12377.
Schmidt, V., Skokan, R., Depaepe, T., Kurtović, K., Haluška, S., Vosolsobě, S., Vaculíková, R., Pil, A., Dobrev, P.I., Motyka, V., et al., 2024. Phytohormone profiling

in an evolutionary framework. Nat. Commun. 15, 3875. https://doi.org/10.1038/s41467-024-47753-z.
Schneider, C.A., Rasband, W.S., Eliceiri, K.W., 2012. NIH Image to ImageJ: 25 years of image analysis. Nat. Methods 9, 671–675. https://doi.org/10.1038/nmeth.2089.
Shibata, M., Oikawa, K., Yoshimoto, K., Kondo, M., Mano, S., Yamada, K., Hayashi, M., Sakamoto, W., Ohsumi, Y., Nishimura, M., 2013. Highly oxidized peroxisomes are selectively degraded via autophagy in *Arabidopsis*. Plant. Cell. 25, 4967–4983. https://doi.org/10.1105/tpc.113.116947.
Stöckle, D., Reyes-Hernández, B.J., Barro, A.V., Nenadić, M., Winter, Z., Marc-Martin, S., Bald, L., Ursache, R., Fujita, S., Maizel, A., et al., 2022. Microtubule-based perception of mechanical conflicts controls plant organ morphogenesis. Sci. Adv. 8, eabm4974. https://doi.org/10.1126/sciadv.abm4974.
Su, T., Wang, P., Li, H., Zhao, Y., Lu, Y., Dai, P., Ren, T., Wang, X., Li, X., Shao, Q., et al., 2018. The *Arabidopsis* catalase triple mutant reveals important roles of catalases and peroxisome-derived signalling in plant development. J. Integr. Plant. Biol. 60, 591–607. https://doi.org/10.1111/jipb.12649.
Talarico, E., Greco, E., Araniti, F., Chiappetta, A., Bruno, L., 2025. Non-CG DNA methylation regulates root stem cell niche maintenance, auxin signalling, and ROS homeostasis in *Arabidopsis* under cadmium stress. Plants 14, 2838. https://doi.org/10.3390/plants14182838.
Tsukagoshi, H., Busch, W., Benfey, P.N., 2010. Transcriptional regulation of ROS controls transition from proliferation to differentiation in the root. Cell 143, 606–616. https://doi.org/10.1016/j.cell.2010.10.020.
Tyagi, S., Singh, K., Upadhyay, S.K., 2021. Molecular characterization revealed the role of catalases under abiotic and arsenic stress in bread wheat (*Triticum aestivum* L.). J. Hazard. Mater. 403, 123585. https://doi.org/10.1016/j.jhazmat.2020.123585.
Vaccarella, E., Piacentini, D., Falasca, G., Canepari, S., Massimi, L., 2023. In-vivo exposure of a plant model organism for the assessment of the ability of PM samples to induce oxidative stress. Sci. Total. Environ. 900, 165694. https://doi.org/10.1016/j.scitotenv.2023.165694.
Yang, Z., Mhamdi, A., Noctor, G., 2019. Analysis of catalase mutants underscores the essential role of CATALASE2 for plant growth and day length-dependent oxidative signalling. Plant. Cell. Environ. 42, 688–700. https://doi.org/10.1111/pce.13453.
Yuan, H.M., Huang, X., 2016. Inhibition of root meristem growth by cadmium involves nitric oxide-mediated repression of auxin accumulation and signalling in *Arabidopsis*. Plant. Cell. Environ. 39, 120–135. https://doi.org/10.1111/pce.12597.
Yuan, H.M., Liu, W.C., Lu, Y.T., 2017. CATALASE2 coordinates SA-mediated repression of both auxin accumulation and JA biosynthesis in plant defenses. Cell. Host Microbe 21, 143–155. https://doi.org/10.1016/j.chom.2017.01.007.
Zafar, S.A., Hameed, A., Ashraf, M., Khan, A.S., Li, X., Siddique, K.H., 2020. Agronomic, physiological and molecular characterization of rice mutants revealed the key role of reactive oxygen species and catalase in high-temperature stress tolerance. Funct. Plant. Biol. 47, 440–453. https://doi.org/10.1071/FP19246.
Zaheer, M.S., Rizwan, M., Aijaz, N., Hameed, A., Ikram, K., Ali, H.H., Niaz, Y., Aslam, H. M.U., Manoharadas, S., Riaz, M.W., et al., 2024. Investigating the synergistic effects of biochar, trans-zeatin riboside, and *Azospirillum brasilense* on soil improvement and enzymatic activity in water-stressed wheat. BMC Plant. Biol. 24, 314. https://doi.org/10.1186/s12870-024-05038-z.
Zhang, Y., Ji, T.T., Li, T.T., Tian, Y.Y., Wang, L.F., Liu, W.C., 2020. Jasmonic acid promotes leaf senescence through MYC2-mediated repression of CATALASE2 expression in *Arabidopsis*. Plant. Sci. 299, 110604. https://doi.org/10.1016/j.plantsci.2020.110604.
Zhang, Y., Wang, L.F., Li, T.T., Liu, W.C., 2021. Mutual promotion of *LAP2* and *CAT2* synergistically regulates plant salt and osmotic stress tolerance. Front. Plant. Sci. 12, 672672. https://doi.org/10.3389/fpls.2021.672672.